Temperature-dependent electrical properties of HgSe†

S. L. Lehoczky, J. G. Broerman, Donald A. Nelson, and Charles R. Whitsett
McDonnell Douglas Research Laboratories, McDonnell Douglas Corporation, St. Louis, Missouri 63166
(Received 3 October 1973)

The electrical conductivity and Hall coefficient between 4.2 and 300 K were measured for single-crystalline samples of the zero-gap semiconductor mercury selenide. The samples had extrinsic electron concentrations ranging from 3.6×10^{16} to 4×10^{18} cm^{-3}. The temperature dependences of the band parameters were obtained by fitting to the Hall-coefficient data a band model based upon the full Kane theory with higher-band corrections. The least-squares fit was obtained for a Γ_6-Γ_8 energy gap which decreased from 0.22 eV at 4.2 K to 0.061 eV at 300 K, an interband-momentum-matrix element which increased slightly from 7.2×10^{-8} eV cm at 4.2 K to 7.6×10^{-8} eV cm at 300 K, an effective hole mass of $0.78m_0$, and a valence-band overlap of the conduction band by 5.0 meV. A variational calculation of the electron mobility between 4.2 and 300 K was performed for each HgSe crystal. The limiting scattering mechanisms were taken to be inter- and intraband longitudinal-optical-phonon scattering, electron-hole scattering, acoustic-phonon scattering, and scattering by charged and neutral defects. The calculations included the properly mixed s and p wave functions, the effects of higher bands on the density of states, the temperature dependence of the band parameters, and the anomalous dielectric function associated with the symmetry-induced zero-gap band structure. The results of the calculations for both the temperature and concentration dependences of the electron mobility are in good agreement with experiment for values of the Szigeti effective charge e_s^* (0.76) and the transverse-optic temperature Θ_T (173 K) which were deduced from optical and acoustical data. At temperatures below about 50 K the electron scattering mainly is by ionized donors and neutral defects. At higher temperatures the electron mobility is limited primarily by longitudinal-optical-phonon scattering. Acoustic-phonon scattering is negligible at all temperatures. An anomalous minimum in the electron mobility near 110 K was observed in mercury selenide that was allowed to sit for a few months at room temperature after having been annealed in vacuum.

I. INTRODUCTION

Mercury selenide (HgSe), along with α-Sn,[1] HgTe,[2] β-HgS,[3] and Cd_3As_2,[4] belongs to a class of materials which have identically zero direct energy gaps and are therefore perfect semimetals. Even though there was never any experimental evidence to support the view, it was widely maintained until past 1960 that HgSe is an intermediate band-gap semiconductor. This was in accord with the prevailing ideas on the trends of band gaps in the progression from the group-IV elements through the III-V to the II-VI compounds, and often quoted for HgSe was an energy gap value of 0.7 eV predicted in 1954 by Goodman[5] in his note on semiconducting compounds and the scale of electronegativities. Thus, many of the early analyses assumed that high impurity concentrations masked the intrinsic electrical properties of HgSe, and various donor levels and impurity-band schemes were postulated.[6,7]

The first major step towards an understanding of the band structure of HgSe was taken by Harman and Strauss,[8] who fitted 77- and 300-K Hall-coefficient data for a large number of HgSe samples with the Kane two-band model for InSb.[9] They concluded that Kane's small-k approximation worked well for HgSe, but that there must be a second valence band which overlapped the conduction band (by 0.07 eV they estimated). However, the bending up of a valence band sufficiently to overlap the conduction band was considered so unreasonable that the semimetal model for HgSe was not generally accepted. The hurdling of the objections to the semimetal model was made possible by the work of Groves and Paul[1] who proposed the symmetry-induced zero-gap structure for α-Sn, and it was at once realized by them[10] and by Harman *et al.*[11] that the Hg chalcogenides most probably have similar band structures. A schematic representation of this unusual band structure, usually called the inverted band structure, is shown in Fig. 1.

In the inverted band structure, the $s^{1/2}$-like Γ_6 level, which is the conduction band in InSb, has moved to an energy lower than the $p^{3/2}$-like Γ_8 level, which in a normal semiconductor forms the zone-center-degenerate light- and heavy-hole valence bands. The light-hole part of Γ_8, since it is $\vec{k} \cdot \vec{p}$ coupled to Γ_6, inverts to form a small-effective-mass conduction band, while the heavy-hole part of Γ_8 remains a valence band. The resulting degeneracy of the valence-band maximum and the conduction-band minimum can be removed only by reducing the crystal symmetry, and the materials are thus called perfect semimetals or symmetry-induced zero-gap semiconductors.[12]

The compatibility of the inverted band structure

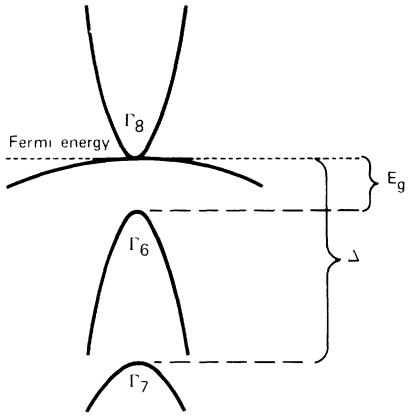

FIG. 1. Simplified model of the band structure near the zone center for a pure symmetry-induced zero-gap semiconductor at absolute zero.

with low-temperature experimental data for HgSe has been well demonstrated, notably for the ionized-impurity-limited electron mobility[13] and for the anisotropy of the beating in the Shubnikov–de Haas oscillations.[14] The low-temperature (4.2 K) band parameters for HgSe are well established by the effective-mass variation with electron concentration.[14,15]

There have been many previous studies of the temperature-dependent electrical properties of HgSe. In 1951 Blum and Regel[16] reported that HgSe is a high-electron-mobility semimetallic compound in which the mobility μ decreases nearly as $T^{-5/2}$. They also reported that HgSe, upon melting, has an abrupt increase of electrical resistivity and that the temperature coefficient of resistivity becomes negative. This unusual transition at the melting temperature has not subsequently been investigated. Tsidil'kovskii[17] studied the magnetic field dependence of the Nernst effect in HgSe, and from the relation $\mu H = 1$ at the magnetic field for the maximum Nernst effect, deduced that $\mu \propto T^{-5/2}$ from 12.0 to 270 K and $\mu \propto T^{-3}$ from 300 to 430 K. For a HgSe crystal with $n = 3.5\times10^{18}$ cm^{-3}, Rodot and Rodot[18] reported that $\mu \propto T^{-2}$. Gobrecht *et al.*[6] found that $\mu \propto T^{-3.5}$ for $n \approx 5\times10^{17}$ cm^{-3} and concluded that the dominant electron scattering mechanism depends upon the electron concentration.

Analyses of the mobility in HgSe have hitherto been based upon the assumption that the electron relaxation time τ is proportional to some power of the electron energy, $\tau = \tau_0 E^r$, where $r = -\frac{1}{2}$ for acoustic-phonon scattering and $r = \frac{1}{2}$ for optical-phonon scattering. Early analyses by Rodot and Rodot[18] and Harman[19] assumed that the conduction band in HgSe is parabolic and implied that scattering by acoustic phonons is dominant. Later, the Kane two-band model for InSb[9] was utilized for the analysis of HgSe and led to the different conclusion that optical-phonon scattering dominates.[20] Indeed, this latter result is compatible with the small value for the deformation potential (~0.7 eV) deduced from analyses of the thermal conductivity of HgSe[21] and the rather high ionicity (0.7–0.8) implied by elastic-constant data.[22] Theoretical investigations of the low-temperature ionized-impurity-limited mobility[23–25] and the temperature-dependent dielectric constant[26,27] in symmetry-induced zero-gap materials strongly suggest, however, that a true characterization of the temperature dependence of the electron mobility in HgSe is possible only in terms of a microscopic theory of electrical conduction.

In this paper, we report a systematic experimental and theoretical investigation of the temperature and concentration dependences of the Hall coefficient and electron mobility of HgSe between 4.2 and 300 K. Until now, the lack of experimental data for the temperature dependence of the conduction-electron concentration for HgSe samples with low donor densities ($< 10^{17}$ cm^{-3}) has precluded a reliable description of the behavior of band parameters at higher temperatures. Here we report Hall-coefficient and mobility data for HgSe for the temperature range from 4.2 to 300 K and for samples with net donor densities that range from 4×10^{18} to 3.6×10^{16} cm^{-3}, almost an order of magnitude lower than obtained in previous investigations. The Hall-coefficient data, when analyzed in terms of the full Kane theory, provide a description of the temperature dependence of the band parameters up to 300 K. To interpret the experimental mobility data, a variational calculation is made based upon a microscopic theory of electrical conduction appropriate for a symmetry-induced zero-gap material. The limiting electron scattering mechanisms are taken to be inter- and intraband polar-optical-phonon scattering, neutral- and charged-defect scattering, electron-hole scattering, and acoustic-phonon scattering. The calculations include the properly mixed s and p wave functions, the effects of higher bands on the density of states, the temperature dependence of the band parameters as determined by the Hall-coefficient data, and the temperature and momentum-transfer dependences of the dielectric function. In Sec. II the preparation of samples and the methods of measuring the Hall coefficient and electron mobility are described. A mathematical model describing the band structure as accurately as possible is developed in Sec. III, and in Sec. IV the fitting of the Hall-coefficient data to determine the temperature variation of the band parameters is described. The screening

of the interactions responsible for scattering is discussed in Sec. V, and in Sec. VI the scattering mechanisms and their contributions to the Boltzmann equation are derived. In Sec. VII, the electron mobility is calculated by means of a variational solution to the Boltzmann equation and compared with experiment. In comparing the calculated mobility with experiment, every effort was made to minimize the number of adjustable parameters. Aside from the inevitable uncertainties regarding the kinds and densities of defects in a given sample, the only important parameter for which there is no experimental measurement is the transverse-optical-phonon frequency, and this can be estimated to within 20% from other measurements.

II. SAMPLE PREPARATION AND EXPERIMENTAL MEASUREMENTS

The samples for this study were cut from single-crystalline HgSe ingots grown by the horizontal traveling molten-zone technique.[28] Spectrographic analyses of representative crystals showed the major metallic impurities to be Cu (0.1–0.7 ppm), Mg (0.5–1.0 ppm), and Si (0–9 ppm). The electron concentration of the as-grown samples ranged from 1.6×10^{18} to 3.5×10^{18} cm^{-3}. To obtain the desired electron concentrations for a given sample, it was subjected to various annealing treatments. These included annealing the samples in the temperature range from 50 to 280 °C in dynamic vacuum ($\approx10^{-6}$ Torr) and in either selenium or mercury vapor corresponding to the equilibrium vapor pressure of the elements for this temperature range. The annealing times varied from a few hours to several days for the vacuum and mercury-vapor annealings and up to several weeks for the selenium-vapor annealings.

The net donor concentrations, deduced from low-temperature (4.2 K) Hall coefficients, and the annealing histories of the specimens are shown in Table I. Identical annealing conditions, especially in the case of vacuum annealings, did not always result in the same net donor concentrations. In some instances, even when the samples were annealed simultaneously, the net donor concentration from sample to sample varied by as much as a factor of 3. This was probably due to wide variations in the concentration of native defects in the ingots. When maintained at room temperature in air, samples which had been annealed to donor concentrations below about 6×10^{17} cm^{-3} showed marked increases with time in their net donor concentrations. In some samples, this increase was by as much as a factor of 3 over a time period of several months. Samples which were allowed to recover in this manner are referred to in Table I as "passive annealed." Similar behavior has been observed for this compound by previous investigators.[29,30] In contrast to the room-temperature behavior, samples maintained at liquid-nitrogen temperature retained their original donor concentrations indefinitely. This behavior and also the variations in the donor concentrations from sample to sample for similar annealing treatments may be indicative of the rather instable nature of the HgSe zinc-blende lattice. For this compound, the ionicity of the selenium-mercury chemical bond, estimated from the elastic constants,[22] is between 0.7 and 0.8. Such a high ionicity is at best only marginally compatible with the Phillips and Van Vechten criterion[31] for a stable zinc-blende lattice.

The Hall coefficient and the electrical conductivity of the samples were measured by using ac potentiometric techniques with phase-sensitive detection. The Hall and conductivity probes were 0.05-mm-diam platinum wires welded to the samples. The current leads were attached with silver paint. The temperature of the samples was monitored by a copper-constantan thermocouple which was in good thermal contact with the samples.

For the low-electron-concentration samples, the period of the Shubnikov–de Haas oscillations at 4.2 K was measured as a function of magnetic field up to 27 kOe. The electron concentrations determined from these period measurements agreed well with those computed from the Hall coefficients. In most cases the difference was less than 2%, which is considerably less than the estimated 4% possible experimental error for the absolute values of the Hall coefficients.

Figures 2 and 3 depict the temperature dependence of the electron concentration for a number of samples with net donor concentrations ranging from 3.6×10^{16} to 5.7×10^{17} cm^{-3}. Sample *AID*, which had a net donor concentration almost a factor of 10 lower than had been previously observed in HgSe, shows nearly an intrinsic behavior down to 20 K. As illustrated in the figures, departure from intrinsic behavior becomes pronounced as the net donor concentration approaches the middle of the 10^{17}-cm^{-3} range. For samples with donor concentrations above 10^{18} cm^{-3}, the electron concentrations were found to be practically independent of temperature between 4.2 and 300 K.

Figures 4 and 5 show the experimental results for the electron mobility in samples *AI* and 52, respectively, as a function of temperature and donor concentration. Figure 6 summarizes the results for samples 51 and 21*JB*. The 4.2-K defect-limited mobilities ranged from 1.46×10^{5} cm^2/V sec for the lowest donor concentration (3.6×10^{16} cm^{-3}) to 2.7×10^{4} cm^2/V sec for the highest donor concentration ($\approx4\times10^{18}$ cm^{-3}). At 300 K the mobilities varied from 2.2×10^{4} to 6.8×10^{3} cm^2/

TABLE I. Annealing histories of HgSe single-crystalline samples. As-grown samples were cooled slowly from the 799 °C melting temperature.

HgSe sample	Annealing history	Electron concentration at 4.2 K (cm^{-3})
AIA	As-grown sample annealed in vacuum at 240 °C for 3 h and at 230 °C for 18 h.	2.10×10^{17}
AIB	HgSe *AIA* subsequently annealed in Se vapor at 255 °C for 12 h.	3.78×10^{17}
AIC	HgSe *AIB* subsequently annealed in vacuum at 230 °C for 48 h.	1.89×10^{17}
AID	HgSe *AIC* subsequently annealed in Se at 200 °C for 24 h, 160 °C for 100 h, 130 °C for 100 h, 90 °C for 150 h, 60 °C for 250 h, and at 25 °C for 300 h.	3.60×10^{16}
AIE	HgSe *AID* subsequently annealed in Hg vapor at 150 °C for 24 h.	3.92×10^{18}
51*A*	As-grown.	1.78×10^{18}
51*B*	HgSe 51*A* subsequently annealed in vacuum at 240 °C for 3 h, 230 °C for 24 h.	5.44×10^{17}
51*C*	HgSe 51*B* subsequently annealed in Se vapor at 250 °C for 12 h.	5.70×10^{17}
51*D*	HgSe 51*C* subsequently annealed in Se vapor at 200 °C for 24 h, 160 °C for 24 h.	4.25×10^{17}
52*A*	As-grown	1.68×10^{18}
52*B*	HgSe 52*A* subsequently annealed in vacuum at 240 °C for 3 h, 230 °C for 24 h.	1.93×10^{17}
52*C*	HgSe 52*B* subsequently annealed in Se vapor at 200 °C for 24 h, 160 °C for 24 h.	1.65×10^{17}
52*D*	HgSe 52*C* subsequently annealed in Hg vapor at 150 °C for 24 h.	3.82×10^{18}
32*B*	After growth, annealed in vacuum at 240 °C for 22 h.	1.52×10^{17}
21*JA*	Previously vacuum annealed sample, annealed in Se vapor at 250 °C for 12 h.	5.00×10^{17}
21*JB*	HgSe 21*JA* subsequently annealed in Hg vapor at 50 °C for 50 h.	1.285×10^{18}
21*L*	Passive annealed.	1.79×10^{18}
21*M*	Passive annealed.	3.65×10^{18}
21*KB*	Passive annealed.	5.32×10^{18}
21*EE*	Passive annealed.	5.64×10^{18}

V sec for the same range of donor concentrations.

The values of the low-temperature (4.2 K) mobilities showed variations from specimen to specimen. For example, the values of the 4.2-K mobilities in samples 52 and 51 for a given donor concentration were consistently about 5% and 25% higher, respectively, than those in sample *AI*. This is due to variations either in the degree of compensation or in the concentration of native defects "frozen" in the specimens during growth. At higher temperatures, the difference in mobility between the sample sequences is much less.

The temperature dependences of the mobility of a number of "passive-annealed" samples are shown in Fig. 7. The most striking feature of these results is the anomalous positive temperature coefficient of the electron mobility in the temperature range 105–150 K.

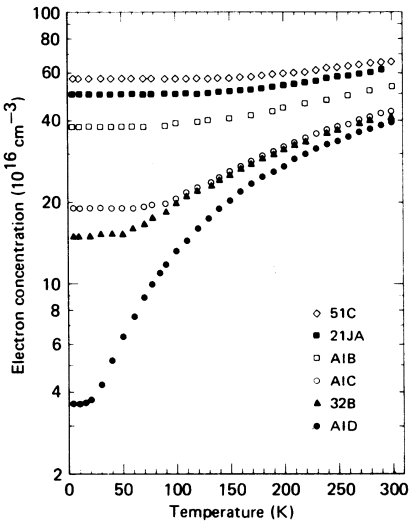

FIG. 2. Electron concentrations calculated from Hall-coefficient data ($n_e = -1/R_H e$) for HgSe samples.

III. BAND STRUCTURE

The calculational model used for the band structure is the full Kane theory[9] in which the $\vec{k}\cdot\vec{p}$ interaction with higher bands is treated by perturbation theory. The conduction-band wave functions are given by

$$|\vec{k}, c, \mu\rangle = e^{i\vec{k}\cdot\vec{r}}|\vec{k}, c, \mu\rangle, \tag{1}$$

$$|\vec{k}, c, \mu\rangle = a\begin{bmatrix}|iS\beta\rangle\\ |iS\alpha\rangle\end{bmatrix} + b\begin{bmatrix}2^{-1/2}|(X-iY)\alpha\rangle\\ -2^{-1/2}|(X+iY)\beta\rangle\end{bmatrix} + c\begin{bmatrix}|Z\beta\rangle\\ |Z\alpha\rangle\end{bmatrix}, \tag{2}$$

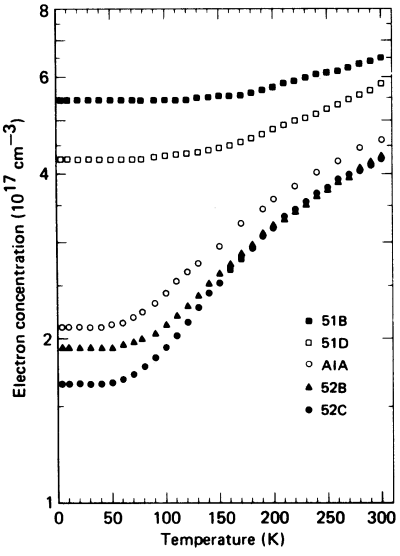

FIG. 3. Electron concentrations calculated from Hall-coefficient data ($n_e = -1/R_H e$) for HgSe samples.

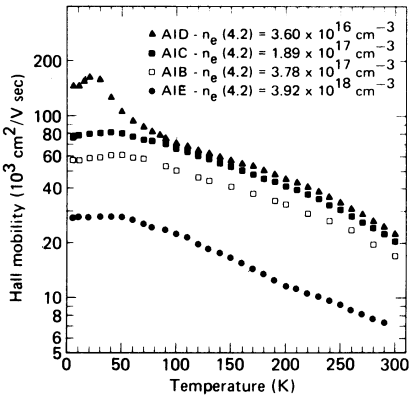

FIG. 4. Electron mobility data for HgSe sample *AI* subjected to a sequence of annealings to achieve different extrinsic electron concentrations. See Table I for annealing history.

and the valence-band wave functions by

$$|\vec{k}, v, \mu\rangle = \begin{bmatrix}2^{-1/2}|(X+iY)\alpha\rangle\\ 2^{-1/2}|(X-iY)\beta\rangle\end{bmatrix}. \tag{3}$$

The quantities X, Y, and Z are the basis set of Γ_{15} referred to a coordinate system with the z axis along $\vec{k}$, and α and β are Pauli spin functions for spin parallel (α) and antiparallel (β) to $\vec{k}$. $|S\rangle$ is the Γ_1 wave function.

The conduction-band eigenvectors are given by

$$a = [\xi'(\xi'+1)(\delta\xi'+1)(\tfrac{3}{2}\delta\xi'+1)]^{1/2}/N, \tag{4}$$

$$b = 3^{-1/2}(\xi'+1)/N, \tag{5}$$

and

$$c = (\tfrac{2}{3})^{1/2}(\xi'+1)(\tfrac{3}{2}\delta\xi'+1)/N. \tag{6}$$

The conduction-band energy is given by

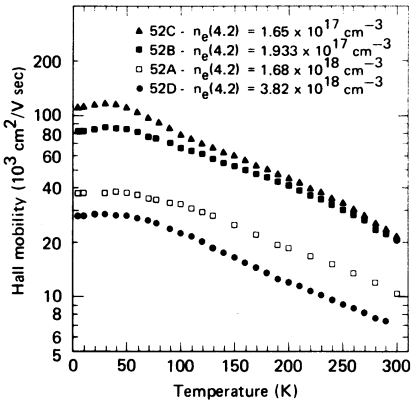

FIG. 5. Electron-mobility data for HgSe sample 52 subjected to a sequence of annealings to achieve different extrinsic electron concentrations. See Table I for annealing history.

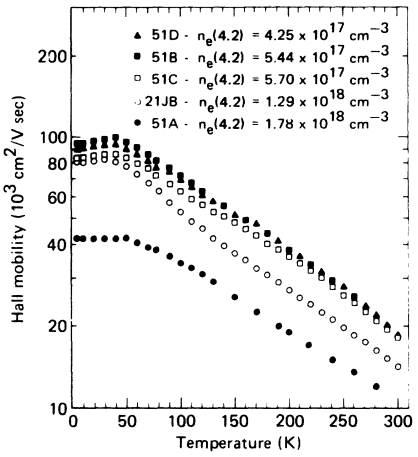

FIG. 6. Electron-mobility data for HgSe sample 51 subjected to a sequence of annealings and for sample 21*JB*. See Table I for annealing histories.

$$E_{k,c}^{*} = E = E' + F(E'), \tag{7}$$

where

$$F(E') = \frac{\hbar^2 k^2}{2m_0}[1 + a^2A' + b^2M + c^2L' + 0.1(b^2 - 2c^2) \times (L' - M - N')], \tag{8}$$

and E' is the largest root of the secular equation

$$E'(E' + E_g)(E' + \Delta) - k^2P^2(E' + \tfrac{2}{3}\Delta) = 0. \tag{9}$$

In these equations m_0 is the free-electron mass, $\xi' = E'/E_g, \delta = E_g/\Delta$, E_g is the Γ_8-Γ_6 energy gap, Δ is the Γ_{15} spin-orbit splitting, N is the square root of the sum of the squares of the numerators of Eqs. (4)–(6), and P is the s-p momentum matrix element defined by Kane. The quantities A', L', M and N' are matrix elements of couplings to higher-lying Γ_{15} and Γ_{12} bands. The expression for $F(E')$, from Seiler, Galazka, and Becker,[14] is a spherical average over the small directional dependence of the conduction-band energy. Small terms which produce asymmetry splitting have been dropped. Seiler, Galazka, and Becker also determined the numerical values of P, E_g, Δ, L', A', M, and N' at 4.2 K for HgSe. The quantity A' is found experimentally to be approximately zero and is not included in the calculations that follow.

In the following we will require expressions for the crystal momentum and conduction-band density of states in terms of the conduction-band energy E. These quantities are most naturally expressed as functions of E'. Although one can develop approximate expressions for E' as a function of E, the least troublesome way to evaluate it numerically is as the limit of a sequence, i.e.,

$$E' = \lim_{n\to\infty} E_n', \tag{10}$$

where $\{E_n'\}$ is the sequence given by the expression $E_n' = E - F(E_{n-1}')$ with $E_0' = E$. In practice, convergence is obtained in a few iterations.

With this in mind, we now solve the secular Eq. (9) for k in terms of the dimensionless function $s(\xi')$ as follows:

$$k = (2\mu_c' m_0 E_g/\hbar^2)^{1/2} s(\xi'), \tag{11}$$

where

$$s(\xi') = \left[\frac{\xi'(\xi'+1)(\delta\xi'+1)}{(\frac{3}{2}\delta\xi'+1)}\right]^{1/2} \tag{12}$$

and μ_c' is the zone-center effective-mass ratio without free-electron or higher-band corrections:

$$\mu_c' = \tfrac{3}{4}\hbar^2 E_g/m_0 P^2. \tag{13}$$

The true zone-center effective-mass ratio μ_c is given by

$$\mu_c = \mu_c'[1 + \tfrac{1}{3}\mu_c'(3 + 2L' + \delta M)]^{-1}. \tag{14}$$

Similarly, the conduction-band density of states per unit volume (neglecting spin) is given by

$$\rho = \frac{(2E_g)^{1/2}(\mu_c' m_0)^{3/2}}{8\pi^3\hbar^3}\lambda(\xi'), \tag{15}$$

where the dimensionless function $\lambda(\xi')$ is defined as

$$\lambda(\xi') = \hbar^3(2E_g)^{-1/2}(\mu_c' m_0)^{-3/2}k^2\frac{dk}{dE}. \tag{16}$$

The exact structure of the valence band of the zinc-blende zero-gap materials is complex. Small antisymmetric spin-orbit couplings to higher bands

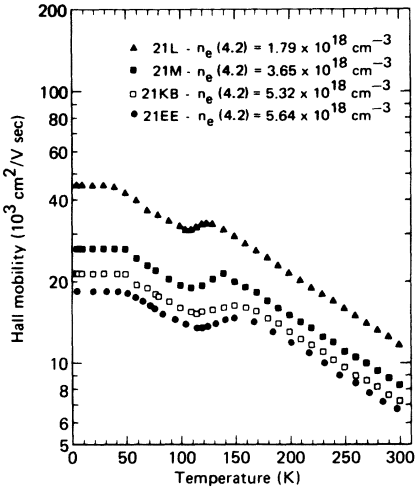

FIG. 7. Electron mobility data for HgSe samples which show an anomalous relative minimum in mobility near 110 K.

split the Γ_8 valence band for $k \neq 0$ so that its maximum is shifted slightly from the zone center to points along the [111] directions. A small overlap with the conduction band is also produced. One can estimate the magnitude of the overlap energy E_{g1} to be 10^{-4}–10^{-3} eV, a value too small to have a significant effect upon scattering in the samples of this study although it should have an observable effect upon the low-temperature Hall coefficient of the lowest concentration samples. The geometrical complications introduced by the Γ_8 valence-band splitting make any serious attempt to treat analytically the resulting microstructure nearly impossible. We therefore approximate the valence band by a spherical parabolic band of mass ratio μ_v overlapping the conduction band by an amount E_{g1}:

$$E_{\vec{k},v} = E_{g1} - (\hbar^2 k^2 / 2\mu_v m_0) . \tag{17}$$

The values obtained for E_{g1} and μ_v must therefore be interpreted with caution.

The parameters L', M, N', μ_v, and E_{g1} may be expected to have only very small temperature dependences because they are determined by bands which lie far above or below Γ_8. The same should also be true of Δ, the Γ_{15} spin-orbit splitting, since it is mainly an atomic property. The Γ_6-Γ_8 energy gap E_g, on the other hand, can be expected to have a large relative temperature dependence since Γ_6 lies very near Γ_8, while the temperature dependence of the s-p momentum matrix element P should be small.

IV. LEAST-SQUARES FIT OF HALL DATA

The conduction-electron concentration as a function of temperature is completely calculable from the band-structure parameters and the concentrations of ionized defects. To the extent that the Hall coefficient is inversely proportional to the electron concentration, it too is determinable. In principle, one could deduce the band-structure parameters from the Hall-coefficient data of a number of samples with different electron concentrations, but in practice this is not feasible because of the large number of parameters and the limitations on the precision with which the absolute magnitude of the Hall coefficient can be measured. However, if one takes as fixed the values for E_g (4.2 K), P (4.2 K), Δ, L', M, and L'-M-N', then by fitting the calculated Hall coefficients to the experimental data, one may determine unambiguously the values for E_g and P at different temperatures as well as the values for E_{g1} and μ_v. We have performed such a fit to the Hall-coefficient data of nine HgSe single crystals (*AIA*, *AIB*, *AIC*, *AID*, 51*B*, 51*D*, 21*JA*, 52*B*, and 52*C*) at 23 different temperatures between 4.2 and 300 K.

The electron concentration was calculated at each temperature and for each sample by solving simultaneously the following set of equations:

$$n_e = \frac{1}{\pi^2}\int_0^\infty k^2 f_0(y, z)\, dk , \tag{18}$$

$$n_h = \frac{1}{2\pi^2}\left(\frac{2\mu_v m_0 k_B T}{\hbar^2}\right)^{3/2} F_{1/2}(E_{g1}/k_B T - z) , \tag{19}$$

and

$$n_e - n_h = N_D - N_A . \tag{20}$$

In Eqs. (18)–(20), n_e is the electron concentration, n_h is the hole concentration, N_D is the donor concentration, N_A is the acceptor concentration, and $F_{1/2}$ is the Fermi function of order $\frac{1}{2}$. The function f_0 is the Fermi-Dirac distribution function,

$$f_0(y, z) = 1/(e^{y-z} + 1) , \tag{21}$$

where $y = E/k_B T$, $z = E_F/k_B T$, and E_F is the Fermi energy. The conduction-band energy E was calculated exactly from Eqs. (7)–(9). The experimental values of the electron concentrations n_{eij} were calculated from the Hall coefficients at temperatures T_j ($j = 1, \ldots, 23$) for samples labeled by the index i ($i = 1, \ldots, 10$). (The indices 9 and 10 both refer to sample *AID*, which was given double weight.) Thus, 230 values of electron concentration n_{eij} were treated as data to be least-squares fit. The parameters Δ, L', M, and L'-M-N' were regarded as fixed, and the values determined by Seiler, Becker, and Galazka[14] were used. The hole mass ratio μ_v and valence-band overlap E_{g1} were treated as parameters which were the same for all samples at all temperatures, but which could be varied to obtain the best fit. The Γ_6-Γ_8 energy gap E_g and the interband-momentum-matrix element P were treated as parameters which were the same for all samples, but which could vary with temperature as required to obtain a fit; the values of E_g and P at 4.2 K were fixed at the values determined by Seiler, Becker, and Galazka. The net donor concentration, $N_D - N_A$, was considered to be a constant for each sample and equal to the 4.2-K electron concentration. If $n_{ei}(T_j)$ is the value of electron-concentration calculated at temperature T_j for the ith sample from Eqs. (18)–(20), then the values of the parameters μ_v, E_{g1}, $(E_g)_j$, and P_j ($j = 2, \ldots, 23$) were found which minimized the expression:

$$\Phi = \sum_{i,j} [\log_{10}(n_{ei}(T_j)) - \log_{10} n_{eij}]^2 . \tag{22}$$

The calculational procedure was begun by assuming a set of initial values for μ_v, E_{g1}, $(E_g)_j$, and P_j and computing Φ. The method of Marquardt[32] then was used to calculate increments of the parameters which would reduce Φ, and this procedure was repeated until a minimum Φ was found. The best fit was obtained with $\mu_v = 0.783$, $E_{g1} = 0.00504$ eV, and with the values for $(E_g)_j$ and P_i given in Table

TABLE II. Values at various temperatures for Γ_6-Γ_8 energy gap E_g and interband momentum matrix element P which give least-squares fit to Hall-coefficient data for HgSe.

Temperature (K)	E_g (eV)	$10^8 P$ (eV cm)
4.2	0.220	7.20
10	0.216	7.21
20	0.208	7.24
30	0.206	7.25
40	0.206	7.25
50	0.204	7.26
60	0.203	7.27
70	0.199	7.30
77.3	0.197	7.32
90	0.187	7.31
100	0.188	7.38
120	0.177	7.40
140	0.159	7.35
160	0.147	7.39
180	0.136	7.46
200	0.128	7.54
220	0.116	7.61
240	0.106	7.69
260	0.091	7.70
270	0.084	7.69
280	0.076	7.67
290	0.068	7.66
300	0.061	7.64

II. In Fig. 8 E_g and P are plotted as functions of temperature. The electron concentrations as functions of temperature calculated from the least-squares-fit parameters are shown for four of the samples in Fig. 9; the agreement with the data shown in Fig. 9 is representative of all the samples.

The values of E_g and P at 4.2 K were fixed, and at this temperature only E_{g1} and μ_v could vary during the fitting. Since the same E_{g1} and μ_v values were used for all temperatures, the values fixed for E_g (4.2 K) and P (4.2 K) had an indirect effect upon the values found for E_g and P at all temperatures. The initial rapid decrease of E_g for temperatures rising from 4.2 to 30 K is mostly a consequence of having fixed the value for E_g (4.2 K) slightly higher than that which would have given the best over-all least-squares fit. A value at 4.2 K of 0.21 eV rather than 0.22 eV would have been better for fitting the Hall-coefficient data and would have resulted in slightly larger values for μ_v and E_{g1}.

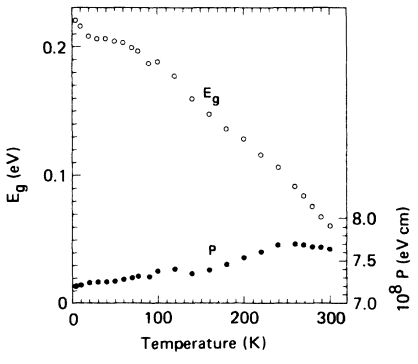

FIG. 8. Values at discrete temperatures of the Γ_6-Γ_8 energy-band gap E_g and the interband-momentum-matrix element P that were determined by a simultaneous least-squares fit to the Hall-coefficient data for nine HgSe crystals.

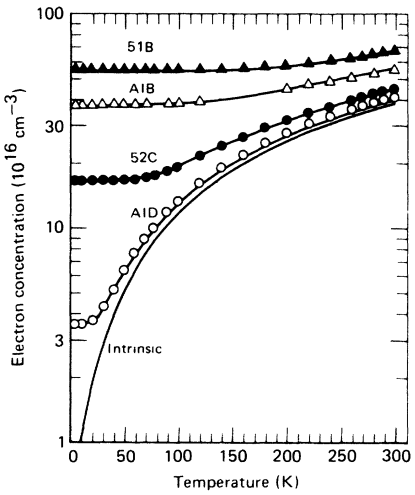

FIG. 9. Least-squares fit to Hall-coefficient data for representative samples. The curves are calculated from the temperature-dependent values for E_g and P shown in Fig. 8. Also shown is the calculated intrinsic curve for HgSe having equal electron and hole concentrations.

The Hall-coefficient data could have been fitted by keeping P the same at all temperatures, and this would have had no significant effect upon the confidence limits for the parameters. Keeping P constant with temperature would have made E_g decrease more rapidly as the temperature increased. On the basis of a statistical analysis of the least-squares fitting, this alternative model with constant P cannot be eliminated. However, the increase of P by about 6% as the temperature increases from 4.2 to 300 K gives a smaller Φ and is not inconsistent with the supposition that P is nearly temperature-independent.

Gelmont and Dyakonov[33] have predicted the existence of quasistationary acceptorlike levels lying a few meV into the conduction-band continuum of the symmetry-induced zero-gap materials. Such acceptor levels would have an influence on the temperature variation of the conduction-electron density similar to that of an overlapping

valence band. Because the present study includes only one sample (*AID*) with a low-temperature Fermi energy (≈15 meV) of the same order of magnitude as the energy (≈ 6 meV) of these acceptor levels, the analysis of the Hall-coefficient data cannot discriminate between these acceptor states and an overlap of the valence band by the conduction band. A larger number of very-low-concentration samples, preferably with Fermi energies lying below the energy of the quasistationary levels, would be required for such an analysis. In fitting the Hall-coefficient data, the overlap E_{g1} has low statistical correlation with the other parameters, and the use of a model which includes the quasistationary states would not significantly change the temperature dependence of the band parameters.

The temperature-dependent values of E_g and P may be used to calculate the cyclotron effective mass, $m^* = \hbar^2 k(dE/dk)^{-1}$, at various temperatures. The effective mass of electrons having the Fermi energy was calculated as a function of electron concentration at 4.2, 100, 200, and 300 K. The ratio of the calculated effective mass to the free electron mass is shown as a function of electron concentration in Fig. 10 for 4.2, 100, and 200 K; the effective-mass ratio at 300 K is shown in Fig. 11. The effective-mass ratios at 4.2 K determined by Whitsett[15] from Shubnikov–de Haas data are shown in Fig. 10, as well as the effective-mass ratios at 100 and 200 K determined by Shalyt and Aliev[34] and by Aliev, Korenblut, and Shalyt[35] from thermoelectric-power data. In Fig. 11 are shown the effective-mass ratios at 300 K determined by Aliev, Korenblut, and Shalyt[35] and those determined by Wright, Strauss, and Harman[29] from room-temperature reflectivity spectra. The agreement between the calculated and experimental effective-mass ratios at 100 and 200 K is striking. The calculated effective masses at 300 K are slightly higher than those deduced by Aliev, Korenblut, and Shalyt and significantly lower than those determined by Wright, Strauss, and Harman. The effective mass values were determined by Wright, Strauss, and Harman from the minima of the reflectivity spectra for samples with a range of electron concentrations, and the values they obtained were sensitive to the value used for the optical dielectric constant. The points shown in Fig. 11 from the work of Aliev, Korenblut, and Shalyt were determined from the magnetic field dependence of the thermoelectric power. The reliability of their method is not as great at 300 K as at lower temperatures because of a number of factors (approximate treatment of degeneracy, approximate treatment of band structure, and relatively lower electron mobilities), and deviations of their data from the curve shown in Fig. 11 should be expected.

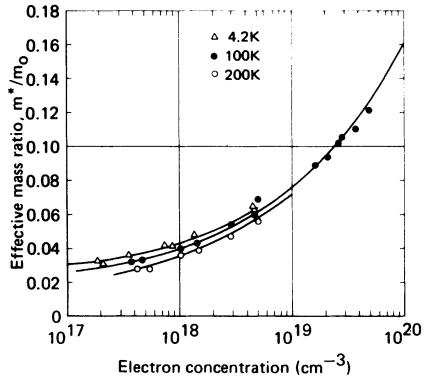

FIG. 10. Curves shown are the calculated cyclotron effective-mass ratios for electrons having the Fermi energy as functions of the conduction-electron concentrations at 4.2, 100, and 200 K. In comparison are shown the data at 4.2 K (△), 100 K (●), and 200 K (○) from Refs. 15, 34, and 35, respectively.

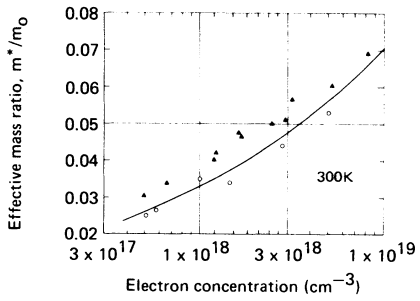

FIG. 11. Curve shown is the calculated cyclotron effective-mass ratio as a function of electron concentration at 300 K for conduction electrons having the Fermi energy. The 300-K data shown for comparison are from Refs. 39 (▲) and 35(○).

A similar decrease in the magnitude of E_g with increasing temperature has been observed by Pidgeon and Groves[36] in HgTe. They observed a temperature coefficient of the band gap almost exactly the same as the average temperature coefficient determined here for HgSe. A decreasing magnitude of the band gap is in contradiction to the prediction of the Brooks-Yu theory,[37] in which the s-like Γ_6 level moves down with respect to the p-like Γ_8 level as the temperature increases. The reason for this discrepancy is not presently understood.

V. SCREENING

Before discussing the mobility-limiting scattering mechanisms, it is necessary to treat the screening functions and their approximations used in the

numerical calculations. We ignore any possible nonadiabatic effects arising from the lattice modes lying within the electron-hole excitation continuum because for the samples of this study the Fermi energies (at temperatures where optical-phonon couplings are important) lie above the lattice modes. The dielectric function is then written as a sum of an electronic part $\epsilon_e(q, \omega)$ and a lattice part $\epsilon_l(q, \omega)$,

$$\epsilon(q, \omega) = \epsilon_e(q, \omega) + \epsilon_l(q, \omega), \tag{23}$$

where

$$\epsilon_l(q, \omega) = \frac{4\pi e^{*2}/\bar{M}v_a}{\omega_T^2 - \omega^2}, \tag{24}$$

and e^*, $\bar{M}$, v_a, and ω_T are, respectively, the effective charge, reduced mass, unit-cell volume, and transverse-optical frequency of the lattice. The quantities e^* and ω_T should be nearly independent of temperature and carrier concentration (as has been observed for HgTe by Grynberg, LeToullec, and Balkanski[38]). We make the usual separation of ϵ_e into inter- and intraband parts,

$$\epsilon_e(q, \omega) = \epsilon_e^{\text{inter}}(q, \omega) + \epsilon_e^{\text{intra}}(q, \omega), \tag{25}$$

and further separate $\epsilon_e^{\text{inter}}$ into a background part ϵ_b, which is the contribution from all interband excitations other than Γ_8-Γ_8 excitations, and $\epsilon_{\Gamma_8}^{\text{inter}}$ which is the contribution from Γ_8-Γ_8 excitations:

$$\epsilon_e^{\text{inter}}(q, \omega) = \epsilon_b(T) + \epsilon_{\Gamma_8}^{\text{inter}}(q, \omega). \tag{26}$$

Because of the large interband energies involved, ϵ_b is independent of q and ω at the small frequencies and momentum transfers of interest in a scattering calculation. We assume that ϵ_b has the same temperature dependence observed by Grynberg, LeToullec, and Balkanski[38] in HgTe, namely,

$$\epsilon_b = \begin{cases} \epsilon_b(300)[1 + \alpha(300 - T)], & T > 100\ \text{K} \\ \epsilon_b(300)[1 + 200\alpha], & T < 100\ \text{K} \end{cases} \tag{27}$$

where $\alpha = 2.22 \times 10^{-3}\ \text{K}^{-1}$.

The evaluation of ϵ^{intra} and $\epsilon_{\Gamma_8}^{\text{inter}}$ is in general difficult. They are given by

$$\epsilon_e^{\text{intra}}(q, \omega) = -\frac{e^2}{\pi^2}\frac{1}{q^2}\sum_{c,v}\int d^3\vec{k}\,\frac{|\langle \vec{k}, n|\, e^{-i\vec{q}\cdot\vec{r}}\,|\vec{k}+\vec{q}, n\rangle|^2}{E_{\vec{k}+\vec{q},n} - E_{\vec{k},n} - \hbar\omega}\,[f(E_{\vec{k}+\vec{q},n}) - f(E_{\vec{k},n})] \tag{28}$$

and

$$\epsilon_{\Gamma_8}^{\text{inter}}(q, \omega) = -\frac{e^2}{\pi^2}\frac{1}{q^2}\mathcal{P}\int d^3\vec{k}\left(\frac{|\langle \vec{k}, v|\, e^{-i\vec{q}\cdot\vec{r}}\,|\vec{k}+\vec{q}, c\rangle|^2}{E_{\vec{k}+\vec{q},c} - E_{\vec{k},v} - \hbar\omega}\,[f(E_{\vec{k}+\vec{q},c}) - f(E_{\vec{k},v})] + (v \rightleftharpoons c)\right), \tag{29}$$

where $\mathcal{P}$ denotes the Cauchy principal value of the integral in Eq. (29). The summation over the band index n in Eq. (28) includes only the Γ_8 conduction and valence bands. Thus, six double integrations are required for every set of values $(N_D - N_A, T, q)$ in order to calculate exactly both the static and dynamic screening functions which enter the mobility calculation. Clearly, some approximations are necessary in order to make the scattering calculations tractable. A number of approximate calculations are available, in either the degenerate or zero-momentum-transfer limits, which can be used without introducing serious errors for most of the electron concentrations and temperatures in this study.

We first consider the static screening. The interband part of ϵ_e has been calculated by Liu and Tosatti[39] for the degenerate case (see Ref. 24 for an estimate of the accuracy of the parabolic approximation used in this calculation). They find

$$\epsilon_e^{\text{inter}}(q, 0) = \epsilon_b(T) + \frac{8e^2\mu_c(T)m_0}{\pi\hbar^2 k_F(T)} \times\left[1 - a'\left(\frac{q}{k_F(T)}\right)^2\right], \tag{30}$$

where $a' \approx \frac{1}{12}$. The second term is the contribution from the $\Gamma_8 \rightleftharpoons \Gamma_8$ excitations. We approximate the dielectric function at all temperatures by this expression, in which $k_F(T)$ is the Fermi momentum of the electron gas evaluated at temperature T. Trial calculations indicate that the approximation is nearly exact for the high-impurity-concentration samples of this study at all temperatures. It underestimates the high-momentum-transfer Γ_8-Γ_8 screening of the low-concentration samples by as much as 10% at high temperatures, which is of no consequence since $\epsilon_{\Gamma_8} \ll \epsilon_b$ at high temperatures. The intraband part has been calculated for degenerate conditions by Broerman, Liu and Pathak[40] and is given by

$$\epsilon_e^{\text{intra}}(q, 0) = (k_{\text{FT}}^2/q^2)[1 - a''(q/k_F)^2 + a'''(q/k_F)^4], \tag{31}$$

where $a'' = 0.47$, $a''' = 0.075$, and k_{FT} is the Fermi-Thomas momentum. The result for a degenerate hole band is identical to this expression, since one can show that, in the parabolic approximation,

$|\langle \vec{k}, c|\, e^{-i\vec{q}\cdot\vec{r}}\,|\vec{k}+\vec{q}, c\rangle|^2$

$$= |\langle \vec{k}, v| e^{-i\vec{q}\cdot\vec{r}} |\vec{k}+\vec{q}, v\rangle|^2 . \quad (32)$$

We approximate the screening at all temperatures by Eq. (31) with k_{FT} given by

$$k_{FT}^2 = (k_{FT}^e)^2 + (k_{FT}^h)^2 , \quad (33)$$

where

$$(k_{FT}^e)^2 = \frac{2e^2}{\pi}(2\mu_c' m_0/\hbar^2)^{3/2} \times (k_B T)^{1/2} \frac{d}{dz}\int_0^\infty \lambda f_0 \, dy \quad (34)$$

and

$$(k_{FT}^h)^2 = \frac{e^2}{\pi}\left(\frac{2\mu_v m_0}{\hbar^2}\right)^{3/2} \times (k_B T)^{1/2} F_{-1/2}\left(\frac{E_{g1}}{k_B T} - z\right) . \quad (35)$$

$F_{-1/2}$ is the Fermi function of order $-\frac{1}{2}$. This expression is exact at zero momentum transfer and overestimates the screening at high momentum transfer.[41] Since at high momentum transfer $\epsilon_e^{intra}(q)$ is relatively small with respect to the total static screening function, the errors introduced by the approximate expressions, Eqs. (31)–(35), should be small.

Next consider the high-frequency dielectric-function appropriate to screening of the electron-optical-phonon interaction. Since the Fermi energy is greater than the longitudinal-optical-phonon energy for temperatures at which optical-phonon scattering is important, except at low temperatures in the lowest electron-concentration sample of the study, the approximation

$$\epsilon_e^{inter}(q, \omega_L) \approx \epsilon_e^{inter}(q, 0) \quad (36)$$

is adequate. The intraband part is more complex. Lindhard[42] has treated two extreme cases depending on the magnitude of the momentum transfer:

$$\epsilon_e^{intra}(q, \omega) \approx \epsilon_e^{intra}(q, 0) \quad (v_0 q \gg \omega) \quad (37a)$$

and

$$\epsilon_e^{intra}(q, \omega) \approx \epsilon_e^{intra}(0, \omega) \quad (v_0 q \ll \omega), \quad (37b)$$

where v_0 is the Fermi velocity for a degenerate distribution or the "average velocity" for a Boltzmann distribution. Because of their small effective mass, the electrons always satisfy the condition of Eq. (37a) for $q > k_F$ and $\omega = \omega_L$. Thus we use Eq. (31) with $k_{FT}^2 = (k_{FT}^e)^2$ for the screening by the electrons. The holes, on the other hand, satisfy the condition of Eq. (37b) for most temperatures and concentrations, with $2v_0 k_F/\omega_L$ approaching unity only at room temperature in the lowest-concentration sample of this study. We therefore make the approximation for the holes

$$\epsilon_{eh}^{intra}(q, \omega_L) = -\frac{\omega_{ph}^2}{\omega_L^2} = -\frac{4\pi m_h e^2/\mu_v m_0}{\omega_L^2} , \quad (38)$$

where ω_{ph} is the hole-plasma frequency. These approximations ignore the antiscreening effects considered by Ehrenreich[43] for the electrons at small momentum transfer and treat the holes as always antiscreening. Because of the large valence-band effective mass, the hole antiscreening is small. The complete high-frequency electronic-dielectric-function is then approximated by

$$\epsilon_e(q, \omega_L) = \epsilon_b(T) + \frac{8e^2\mu_c m_0}{\pi\hbar^2 k_F}[1 - a'(q/k_F)^2] + (k_{FT}^e)^2/q^2[1 - a''(q/k_F)^2 + a'''(q/k_F)^4] - \omega_{ph}^2/\omega_L^2 . \quad (39)$$

As mentioned in the discussion of the static screening, the approximation of Eq. (31) for the electron screening, which was derived in the parabolic approximation with pure $p^{3/2}$ wave functions, tends to overestimate the high-momentum transfer screening. This error becomes serious as E_F becomes much larger than E_g. Because of the relatively small value of ϵ_b and the rapid decrease of E_g with increasing temperature, the theory is not expected to be quantitatively valid at temperatures approaching 300 K for samples with impurity-carrier concentrations above 10^{18} cm^{-3}.

The LO-phonon frequency is determined by the condition $\epsilon(q, \omega) = 0$. Since ϵ is q dependent, there will be some dispersion in the values of $\omega_L(q)$. The dispersion is less than 10% in all samples for the most important range of q ($k_F < q < 2k_F$) and will be ignored. The LO-phonon frequency is then given by

$$\omega_L = \left[\frac{\omega_T^2\epsilon_0^t + \omega_{ph}^2 + [(\omega_T^2\epsilon_0^t + \omega_{ph}^2)^2 - 4\epsilon_\infty^t\omega_{ph}^2\omega_T^2]^{1/2}}{2\epsilon_\infty^t}\right]^{1/2} . \quad (40)$$

The quantities ϵ_0^t and ϵ_∞^t are defined as

$$\epsilon_\infty^t = \epsilon_\infty^b + 8e^2\mu_c m_0/\pi\hbar^2 k_F \quad (41)$$

and

$$\epsilon_0^t = \epsilon_0^b + 8e^2\mu_c m_0/\pi\hbar^2 k_F , \quad (42)$$

where $\epsilon_\infty^b = \epsilon_b$ and

$$\epsilon_0^b = \epsilon_b + \frac{4\pi e^{*2}/\bar{M}v_a}{\omega_T^2} . \quad (43)$$

The validity of Eq. (40) depends upon the Fermi energy being sufficiently large at the temperatures for which LO-phonon scattering is important that ϵ_{Γ_8} has approximately its static value. For n-type HgSe below 300 K, $(\omega_{ph}/\omega_L)^2 \ll 1$, so that a good approximation to Eq. (40) is

$$\omega_L = \omega_T(\epsilon_0^t/\epsilon_\infty^t)^{1/2} . \quad (44)$$

The quantity $\epsilon_0^t(300)$ [which for a high concentration sample is approximately the same as $\epsilon_0^b(300)$] has been measured by Kiriashkina *et al.*[44] to be 25.6. Volkov, Volkov, and Kiriev[45] find $\epsilon_\infty^t(300)$ to be 9 ± 1. From this value for $\epsilon_\infty^t(300)$ and the results of Broerman,[27] we estimate the value of $\epsilon_b(300)$ to be 8.25 ± 1. The ratio $|e^*/\omega_T|$ is then determined by the relation

$$\left(\frac{e^*}{\omega_T}\right)^2 = \frac{\bar{M}v_a}{4\pi}\left[\epsilon_0^b(300) - \epsilon_\infty^b(300)\right]. \tag{45}$$

We are thus left with ω_T as the only undetermined quantity. Szigeti[46] has derived an expression for ω_T in terms of the compressibility β and the high- and low-frequency dielectric constants. His expression does not include anharmonic higher-temperature effects, and its derivation is based upon a deformable-ion model which includes central-force nearest-neighbor interactions only. We therefore believe that the dielectric constants which should enter the Szigeti relation are the low-temperature large-momentum-transfer dielectric functions and should not include the contribution from the $\Gamma_8 \leftrightarrow \Gamma_8$ excitations. In our notation, this relation is then given by

$$\omega_T^2 = \frac{3v_a}{\bar{M}r_0^2}\frac{\left[\epsilon_\infty^b(0)+2\right]}{\left[\epsilon_0^b(0)+2\right]}\frac{1}{\beta}, \tag{46}$$

where r_0 is the nearest-neighbor distance. The low-temperature compressibility β for HgSe is 1.753×10^{-12} cm/dyn.[22] The relation of Eq. (46) ordinarily overestimates ω_T. The experimental value of ω_T for HgTe is 15% lower than that given by Eq. (46), and because of the general similarity of the compounds we assume that the same is true for HgSe. Thus, to obtain ω_T for HgSe, we multiply the result of Eq. (46) by the empirical factor 0.85.

In the calculation of electron mobility, the only dielectric parameter that is allowed to vary is $\epsilon_\infty^t(300)$, and that only within the range of experimental uncertainty (9 ± 1). The remaining dielectric parameters ϵ_b, e^*, and ω_T are then determined by the choice of $\epsilon_\infty^t(300)$. For $\epsilon_\infty^t(300)=9$, values are obtained of 3.92 for e^*/e and 168 K for $\theta_T = \hbar\omega_T/k_B$. For comparison, e^*/e has the values 2.96 for HgTe and 2.35 for CdTe (for a compilation of e^*/e values see Burstein, Pinczuk, and Wallis[47]).

VI. SCATTERING MECHANISMS AND MOBILITY

Polar-optical-phonon scattering, acoustical-phonon scattering, ionized-impurity scattering, and electron-hole scattering will be considered. All other couplings, such as the nonpolar electron–optical-phonon coupling, should be much weaker than these. We ignore multiple scattering effects, such as those considered by Moore,[48] which should be relatively small for the zero-gap band structure.

The field term of the Boltzmann equation for a system driven by a static electric field $\vec{\mathcal{E}}$ is given by

$$\left(\frac{\partial f(\vec{k})}{\partial t}\right)_F = \frac{\mathcal{E}e}{\hbar} f_0' \frac{dE}{dk}\cos\theta, \tag{47}$$

where θ is the angle between $\vec{k}$ and $\vec{\mathcal{E}}$, $f(\vec{k})$ is the perturbed distribution function, and $f_0' = df_0/dE$. We make the usual ansatz for the form of the perturbed distribution function in the conduction band:

$$f(\vec{k}) = f_0 - kc'(E)f_0'\cos\theta \quad (E>0). \tag{48}$$

The very heavy holes are assumed to be nearly unperturbed by the small driving field, so that $f(\vec{k}) \approx f_0(E)$ for $E<0$. This is a very good approximation, since $\mu_v/\mu_c > 30$ at all temperatures.

A. Polar-optical-phonon scattering

The matrix element for the scattering of an electron from a state characterized by wave vector $\vec{k}$, band n, and magnetic substate μ to the state $|\vec{k}+\vec{q}, n', \mu'\rangle$ by a LO phonon of frequency ω_L is given by[43,49]

$$\langle \vec{k}, n, \mu | H | \vec{k}+\vec{q}_\pm, n', \mu'\rangle = \pm \frac{4\pi ie}{v_a}\left(\frac{\hbar}{2\bar{M}G^3\omega_L}\right)^{1/2} \times \frac{e^*}{q_\pm \epsilon_e(q,\omega_L)}\begin{Bmatrix}(\mathfrak{N})^{1/2}\\(\mathfrak{N}+1)^{1/2}\end{Bmatrix}\langle \vec{k}, n, \mu | e^{-i\vec{q}_\pm\cdot\vec{r}} | \vec{k}+\vec{q}_\pm, n', \mu'\rangle. \tag{49}$$

The upper and lower quantities refer to phonon absorption and emission, respectively, and $\mathfrak{N}$ is the number of phonons of energy $\hbar\omega_L = k_B\Theta_L$ at the temperature T; i.e.,

$$\mathfrak{N} = 1/(e^{\Theta_L/T}-1). \tag{50}$$

Both inter- and intraband processes are possible for the zero-gap band-structure, but otherwise the derivation of the contribution of the LO-phonon-scattering mechanism to the Boltzmann equation is straightforward. The expression for ϵ^{intra} of Eq. (31) is an approximation not valid for $q>2k_F$ and will give unphysically large values for the screening if extended beyond this momentum transfer. Since $\epsilon^{\text{intra}} \ll \epsilon_b$ for $q>2k_F$, we set $\epsilon^{\text{intra}}=0$ for $q>2k_F$. The matrix elements required for the scattering calculation have been derived by Broerman[24] and Broerman, Liu, and Pathak.[39] They are given by

$$\frac{1}{2}\sum_{\mu,\mu'}|\langle \vec{k}, c, \mu | e^{-i\vec{q}_\pm\cdot\vec{r}} | \vec{k}+\vec{q}_\pm, c, \mu'\rangle|^2 = \sum_{n=0}\rho_n^\pm(E_k, E_{\vec{k}+\vec{q}_\pm})\left|\frac{\vec{k}\cdot(\vec{k}+\vec{q}_\pm)}{k|\vec{k}+\vec{q}_\pm|}\right|^n \tag{51}$$

and

$$\frac{1}{2}\sum_{\mu,\mu'}|\langle\vec{k},c,\mu|e^{-i\vec{q}_\pm\cdot\vec{r}}|\vec{k}+\vec{q}_\pm,v,\mu'\rangle|^2 = \frac{(b+\sqrt{2}\,c)^2}{4}\left|\frac{\vec{k}\times\vec{q}_\pm}{k|\vec{k}+\vec{q}_\pm|}\right|^2, \quad (52)$$

where

$$\rho_0^\pm = (aa_\pm)^2 + \tfrac{1}{4}(bb_\pm)^2 - bb_\pm\frac{(bc_\pm+cb_\pm)}{\sqrt{2}} + \frac{(bc_\pm+cb_\pm)^2}{2}, \quad (53)$$

$$\rho_1^\pm = 2(aa_\pm)(bb_\pm+cc_\pm), \quad (54)$$

and

$$\rho_2^\pm = \tfrac{3}{4}(bb_\pm)^2 + bb_\pm\frac{(bc_\pm+cb_\pm)}{\sqrt{2}} + 2(bb_\pm)(cc_\pm) - \tfrac{1}{2}(bc_\pm+cb_\pm)^2 + (cc_\pm)^2. \quad (55)$$

The ± subscripts refer to the evaluation of the quantity at $E\pm\hbar\omega_L$, and a, b, and c are defined by Eqs. (4)–(6).

One then obtains for the contribution to the Boltzmann equation from LO-phonon scattering the following:

$$\left(\frac{\partial f(\vec{k})}{\partial t}\right)_{\rm LO} = -\frac{4\pi(e_c^*e)^2\mu_c' m_0}{\hbar^2\bar{M}v_a\omega_L\lambda sE_g}f_0'\cos\theta L_{\rm LO}(c'), \quad (56)$$

where

$$L_{\rm LO}(c') = E_g\{(f_+/f_0)(\mathfrak{N}+1)(c_+'R_+ - c'S_+) + (f_-/f_0)\mathfrak{N}[h(E)(c_-'R_- - c'S_-) - (1-h(E))c'\Sigma]\} \quad (57)$$

and

$$h(E) = \begin{cases}1 & (E>\hbar\omega_L)\\ 0 & (E<\hbar\omega_L).\end{cases} \quad (58)$$

The quantity e_C^*, the Callen (or interaction) effective charge, is given by

$$e_C^* = e^*/\epsilon_\infty^t(T). \quad (59)$$

The other functions are defined as follows:

$$R_\pm = \lambda\lambda_\pm(s/s_\pm)\sum_{n=0}^{2}\rho_n^\pm(V_n^\pm(x)+V_n'^\pm(x)), \quad (60)$$

$$S_\pm = \lambda\lambda_\pm\sum_{n=0}^{2}\rho_n^\pm(U_n^\pm(x)+U_n'^\pm(x)), \quad (61)$$

and

$$x = \begin{cases}1 & [|s_\pm - s| > 2s(z)]\\ [s^2+s_\pm^2-4s^2(z)]/2ss_\pm & [|s_\pm - s| < 2s(z) < |s_\pm + s|]\\ -1 & [|s_\pm + s| < 2s(z)]\end{cases}. \quad (62)$$

The functions $U_i^\pm$ and $V_i^\pm$ are given by

$$U_i^\pm(x) = s^2[(s_\pm^2+s^2)W_i^\pm(x) - 2ss_\pm W_{i+1}^\pm(x)] \quad (63)$$

and

$$V_i^\pm(x) = s^2[(s_\pm^2+s^2)W_{i+1}^\pm(x) - 2ss_\pm W_{i+2}^\pm(x)], \quad (64)$$

where

$$W_0^\pm(x) = \frac{1}{4A_\pm C_\pm - B_\pm^2}\left[\frac{2A_\pm+B_\pm}{A_\pm+B_\pm+C_\pm} - \frac{2A_\pm x+B_\pm}{A_\pm x^2+B_\pm x+C_\pm} + 2A_\pm W_\pm(x)\right], \quad (65)$$

$$W_1^\pm(x) = \frac{1}{4A_\pm C_\pm - B_\pm^2}\left[\frac{B_\pm x+2C_\pm}{A_\pm x^2+B_\pm x+C_\pm} - \frac{B_\pm+2C_\pm}{A_\pm+B_\pm+C_\pm} - B_\pm W_\pm(x)\right], \quad (66)$$

$$W_2^\pm(x) = \frac{1}{A_\pm(4A_\pm C_\pm - B_\pm^2)}\left[\frac{B_\pm^2-2A_\pm C_\pm+B_\pm C_\pm}{A_\pm+B_\pm+C_\pm} - \frac{(B_\pm^2-2A_\pm C_\pm)x+B_\pm C_\pm}{A_\pm x^2+B_\pm x+C_\pm} + 2A_\pm C_\pm W(x)\right], \quad (67)$$

$$W_3^\pm(x) = \frac{1}{A_\pm}\left[\frac{1}{2A_\pm}\ln\left|\frac{A_\pm+B_\pm+C_\pm}{A_\pm x^2+B_\pm x+C_\pm}\right| - \frac{B_\pm}{2A_\pm}W_\pm(x) - C_\pm W_1^\pm(x) - B_\pm W_2^\pm(x)\right], \quad (68)$$

$$W_4^\pm(x) = \frac{1}{A_\pm}\left[\frac{1}{(A_\pm+B_\pm+C_\pm)} - \frac{x^3}{(A_\pm x^2+B_\pm x+C_\pm)} - 3C_\pm W_2^\pm(x) - 2B_\pm W_3^\pm(x)\right], \quad (69)$$

and

$$W_\pm(x) = \begin{cases}\dfrac{1}{(B_\pm^2-4A_\pm C_\pm)^{1/2}}\ln\left|\dfrac{(1-P_\pm)(x-Q_\pm)}{(1-Q_\pm)(x-P_\pm)}\right| & (B_\pm^2>4A_\pm C_\pm)\\ \dfrac{2}{(4A_\pm C_\pm-B_\pm^2)^{1/2}}\left[\tan^{-1}\left(\dfrac{2A_\pm+B_\pm}{(4A_\pm C_\pm-B_\pm^2)^{1/2}}\right)-\tan^{-1}\left(\dfrac{2A_\pm x+B_\pm}{(4A_\pm C_\pm-B_\pm^2)^{1/2}}\right)\right] & (B_\pm^2<4A_\pm C_\pm).\end{cases} \quad (70)$$

The functions $A_\pm$, $B_\pm$, $C_\pm$, $P_\pm$, and $Q_\pm$ are given by

$$A_\pm = \frac{4s^2s_\pm^2}{s^2(z)}\left[\frac{g_\infty^2 a'''}{s^2(z)} - (1-\epsilon_b/\epsilon_\infty^t)a'\right], \quad (71)$$

$$B_{\pm} = -2ss_{\pm}\left\{\frac{2(s_{\pm}^2+s^2)}{s^2(z)}\left[\frac{g_{\infty}^2}{s^2(z)}a''' - (1-\epsilon_b/\epsilon_{\infty}^t)a'\right]+1-\frac{g_{\infty}^2}{s^2(z)}a''\right\}, \tag{72}$$

$$C_{\pm} = (s_{\pm}^2+s^2)\left\{\frac{g_{\infty}^2}{s^2+s_{\pm}^2}+1-\frac{g_{\infty}^2}{s^2(z)}a''+\frac{(s_{\pm}^2+s^2)}{s^2(z)}\left[\frac{g_{\infty}^2}{s^2(z)}a''' - (1-\epsilon_b/\epsilon_{\infty}^t)a'\right]\right\}, \tag{73}$$

$$P_{\pm} = [-B_{\pm}+(B_{\pm}^2-4A_{\pm}C_{\pm})^{1/2}]/2A_{\pm}, \tag{74}$$

and

$$Q_{\pm} = [-B_{\pm}-(B_{\pm}^2-4A_{\pm}C_{\pm})^{1/2}]/2A_{\pm}, \tag{75}$$

where

$$g_{\infty}^2 = \hbar^2(k_{FT}^e)^2/2\mu_c' m_0 E_g \epsilon_{\infty}^t . \tag{76}$$

The functions $V_i'^{\pm}$ and $U_i'^{\pm}$ are given by

$$V_0'^{\pm}(x) = -\frac{s}{2s_{\pm}}\left[x+1+\frac{s^2+s_{\pm}^2}{2ss_{\pm}}\ln\left|\frac{s^2+s_{\pm}^2-2ss_{\pm}x}{(s+s_{\pm})^2}\right|\right], \tag{77}$$

$$V_1'^{\pm}(x) = -\frac{1}{2s_{\pm}^2}\left[\frac{(s^2+s_{\pm}^2-2ss_{\pm}x)^2-(s+s_{\pm})^4}{8ss_{\pm}}+(s^2+s_{\pm}^2)(1+x)+\frac{(s^2+s_{\pm}^2)^2}{4ss_{\pm}}\ln\left|\frac{s^2+s_{\pm}^2-2ss_{\pm}x}{(s+s_{\pm})^2}\right|\right], \tag{78}$$

$$V_2'^{\pm}(x) = \frac{1}{16s^2s_{\pm}^4}\left(\tfrac{1}{3}[(s^2+s_{\pm}^2-2ss_{\pm}x)^3-(s+s_{\pm})^6]-\tfrac{3}{2}(s^2+s_{\pm}^2)[(s^2+s_{\pm}^2-2ss_{\pm}x)^2-(s+s_{\pm})^4]\right.$$
$$\left.-6ss_{\pm}(s^2+s_{\pm}^2)^2(x+1)-(s^2+s_{\pm}^2)^3\ln\left|\frac{s^2+s_{\pm}^2-2ss_{\pm}x}{(s+s_{\pm})^2}\right|\right), \tag{79}$$

$$U_0'^{\pm}(x) = -\frac{s}{2s_{\pm}}\ln\left|\frac{s^2+s_{\pm}^2-2ss_{\pm}x}{(s+s_{\pm})^2}\right|, \tag{80}$$

$$U_1'^{\pm}(x) = V_0'^{*}(x), \tag{81}$$

and

$$U_2'^{\pm}(x) = V_1'^{\pm}(x). \tag{82}$$

The interband part Σ in Eq. (57) is given by

$$\Sigma = \lambda\sigma[\psi(x)+\psi'(x)]/\gamma, \tag{83}$$

where

$$\sigma = \gamma^{-1/2}[\beta(\Theta_L/T-y)]^{1/2}. \tag{84}$$

Here γ is the ratio μ_c'/μ_v, and $\beta = k_B T/E_g$. The functions ψ and ψ' are given by

$$\psi(x) = \tfrac{1}{4}(b+\sqrt{2}\,c)^2 s^2\{(s^2+\sigma^2)[W_0(x)-W_2(x)]+2s\sigma[W_3(x)-W_1(x)]\} \tag{85}$$

and

$$\psi'(x) = \tfrac{1}{4}(b+\sqrt{2}\,c)^2\frac{s}{2\sigma}\left\{\left[\frac{(\sigma^2+s^2)^2}{(2\sigma s)^2}-1\right]\ln\left|\frac{\sigma^2+s^2-2\sigma sx}{(\sigma+s)^2}\right|+\frac{1}{(2\sigma s)^2}\left[\frac{(\sigma^2+s^2-2\sigma sx)^2}{2}-\frac{(\sigma+s)^4}{2}+4\sigma s(\sigma^2+s^2)(x+1)\right]\right\}, \tag{86}$$

where x and the $W_i(x)$ are calculated by everywhere replacing $s_{\pm}$ by σ in Eqs. (62) and (65)–(75).

B. Acoustic-phonon scattering

Zawadzki and Szymánska[50] have recently investigated the interaction of acoustic phonons with electrons which have wave functions containing p-like components. Their results indicate that the interaction of such electrons with acoustic phonons differs from that of s-like electrons in two major respects. First, the symmetry of the wave function allows a nonvanishing coupling to the transverse modes which can be comparable in strength to the coupling to the longitudinal mode. Second, instead of the single deformation potential of the free-electron theory, five independent irreducible

matrix elements are necessary to characterize the couplings. In the following we present the results of Zawadzki and Szymánska, modified to our case of Γ_8 symmetry of the conduction-band minimum.

The Boltzmann equation in the elastic approximation is given by

$$\left(\frac{\partial f(\vec{k})}{\partial t}\right)_{\text{ac.}} = \frac{2k_B T E_0^2}{\pi\hbar^5 d v_l^2}(\mu_c' m_0)^2 E_g \lambda s \times [F_l + (v_l/v_t)^2 F_t] f_0' \cos\theta\, c'(E), \quad (87)$$

where d is the mass density of the material, and v_l and v_t are the longitudinal and transverse velocities of sound, respectively. The quantity E_0 is the ordinary longitudinal coupling of phonons to the component of the wave function belonging to the s-like Γ_6 band with zone-center wave function $|S\rangle$:

$$E_0 = \frac{\hbar^2}{3m_0}\frac{1}{v_a}\int_{v_a}(\vec{\nabla}S)^2 d^3\vec{r}. \quad (88)$$

The longitudinal and transverse scattering functions, F_l and F_t, are given by

$$F_l = A_1^2 + \tfrac{2}{3}(A_1A_2 + A_4) + \tfrac{1}{2}(2A_1A_3 + A_2^2 - A_4) + \tfrac{4}{5}A_2A_3 + \tfrac{1}{3}A_3^2 \quad (89)$$

and

$$F_t = (E_1^2/E_0^2)(B_1 + \tfrac{2}{3}B_2 + \tfrac{1}{2}B_3 + \tfrac{2}{5}B_4 + \tfrac{1}{3}B_5 + B_6), \quad (90)$$

where

$$A_1 = a^2 + (E_1/E_0)(\tfrac{1}{2}b^2) + (E_2/E_0)(c^2 + \tfrac{1}{2}b^2), \quad (91)$$

$$A_2 = -(E_1/E_0)(c^2 + \tfrac{1}{2}b^2) + (E_2/E_0)(5c^2 + \tfrac{1}{2}b^2), \quad (92)$$

$$A_3 = 4(E_2/E_0)(c^2 - \tfrac{1}{2}b^2), \quad (93)$$

$$A_4 = (E_1/E_0)^2 b^2 c^2, \quad (94)$$

$$B_1 = \tfrac{1}{4}b^4, \quad (95)$$

$$B_2 = -b^2[b(b+\sqrt{2}\,c) + \tfrac{1}{4}b^2 - (b + c/\sqrt{2})^2], \quad (96)$$

$$B_3 = b^2[(b+\sqrt{2}\,c)^2 + b(b+\sqrt{2}\,c) - 2(b+c/\sqrt{2})(b+\sqrt{2}\,c) - (b+c/\sqrt{2})^2], \quad (97)$$

$$B_4 = 2b^2(b + c/\sqrt{2})(b+\sqrt{2}\,c), \quad (98)$$

$$B_5 = -b^2(b+\sqrt{2}\,c)^2, \quad (99)$$

and

$$B_6 = \tfrac{1}{2}[b^2c^2 + \tfrac{1}{3}(c^2 - \tfrac{1}{2}b^2)^2]. \quad (100)$$

The matrix elements E_1 and E_2 are defined by

$$E_1 = \frac{\hbar^2}{m_0}\frac{1}{v_a}\int_{v_a}\left(\frac{\partial X}{\partial x}\right)^2 d^3\vec{r} \quad (101)$$

and

$$E_2 = \frac{\hbar^2}{m_0}\frac{1}{v_a}\int_{v_a}\left(\frac{\partial X}{\partial y}\right)^2 d^3\vec{r}. \quad (102)$$

The simplifying approximations,

$$\frac{\hbar^2}{m_0}\frac{1}{v_a}\int_{v_a}\left(\frac{\partial X}{\partial x}\right)\left(\frac{\partial Y}{\partial y}\right) d^3\vec{r} = E_1 \quad (103)$$

and

$$\frac{\hbar^2}{m_0}\frac{1}{v_a}\int_{v_a}\left(\frac{\partial X}{\partial y}\right)\left(\frac{\partial Y}{\partial x}\right) d^3\vec{r} = E_2, \quad (104)$$

have been made in the derivation of these results. Zawadzki and Szymánska point out that in the hydrogenic approximation $E_1/E_0 = \frac{9}{20}$ and $E_2/E_0 = \frac{3}{20}$, while in the empty-lattice approximation $E_1/E_0 = 1$ and $E_2/E_0 = 0$. The correct values lie somewhere between these sets.

C. Ionized-impurity scattering

The scattering of electrons on ionized impurities screened by the random-phase-approximation (RPA) dielectric function of Eqs. (30) and (31) has been treated by Broerman[24] and Broerman, Liu and Pathak.[40] We will adopt their results intact with one additional approximation. The q-dependent terms in the static dielectric function produce only small effects in the mobility of samples in the electron-concentration range of this study because they are masked by the large value of ϵ_0^b. We ignore the q-dependent terms and thereby obtain for the contribution to the Boltzmann equation from the ith type of ionized defect

$$\left(\frac{\partial f(\vec{k})}{\partial t}\right)_{\text{i.d.}} = \frac{\pi N_i Z_i^2 e^4 \lambda}{\hbar(\epsilon_0^t)^2 E_g s^3}\Phi f_0' \cos\theta\, c'(E), \quad (105)$$

where N_i is the density of defects of charge $Z_i e$. The scattering function Φ is given by

$$\Phi = \sum_{n=0}^{2}\pi_n\phi_n, \quad (106)$$

where

$$\phi_0 = \ln[(g_0^2 + 4s^2)/g_0^2] - 4s^2/(g_0^2 + 4s^2), \quad (107)$$

$$\phi_1 = \frac{g_0^2 + s^2}{s^2}\ln\left(\frac{g_0^2 + 4s^2}{g_0^2}\right) - \frac{4(g_0^2 + 3s^2)}{(g_0^2 + 4s^2)}, \quad (108)$$

$$\phi_2 = \frac{g_0^2}{2s^2}\left[-\frac{4(g_0^2 + s^2)}{g_0^2} + \frac{(g_0^2 + 2s^2)(3g_0^2 + 2s^2)}{2s^2 g_0^2} \times \ln\left(\frac{g_0^2 + 4s^2}{g_0^2}\right) - \frac{2(g_0^2 + 2s)^2}{g_0^2(g_0^2 + 4s^2)}\right], \quad (109)$$

$$\pi_0 = a^4 + \tfrac{1}{4}b^4 - \sqrt{2}\,b^3c + 2b^2c^2, \quad (110)$$

$$\pi_1 = 2a^2(b^2 + c^2), \quad (111)$$

$$\pi_2 = \tfrac{3}{4}b^4 + \sqrt{2}\,b^3c + c^4, \quad (112)$$

and

$$g_0^2 = \hbar^2[(k_{FT}^e)^2 + (k_{FT}^h)^2]/2\mu_c' m_0 E_g \epsilon_0^t. \quad (113)$$

These results are equivalent to setting $a' = a'' = a''' = 0$ in the expressions for the dielectric function in Eqs. (30) and (31).

D. Electron-hole scattering

In the usual treatment of electron-hole scattering, the hole is regarded as a fixed charge of magnitude $+e$, and $N_i Z_i^2$ in Eq. (105) (for ionized-defect scattering) is replaced by n_h, the density of holes. In reality, the hole is not a localized charge, and the situation is much more complicated. The probability of an electron in state $|\vec{k}_1, c\rangle$ being scattered by the ensemble of electrons in the valence band to state $|\vec{k}_1+\vec{q}, c\rangle$ is given[51] in the first Born approximation by

$$W_{\vec{k}_1,c;\vec{k}_1+\vec{q},c} = \frac{2\pi}{\hbar}\left[\frac{4\pi e^2}{\epsilon(q,0)q^2}\right]^2 |\langle \vec{k}_1, c| e^{-i\vec{q}\cdot\vec{r}_1}|\vec{k}_1+\vec{q}, c\rangle|^2 f_{\vec{k}_1,c}(1-f_{\vec{k}_1+\vec{q},c})\sum_{\vec{k}_2} |\langle \vec{k}_2, v| e^{i\vec{q}\cdot\vec{r}_2}|\vec{k}_2-\vec{q}, v\rangle|^2 f_{\vec{k}_2,v}(1-f_{\vec{k}_2-\vec{q},v})$$

$$= \frac{2\pi}{\hbar}\left[\frac{4\pi e^2}{\epsilon(q,0)q^2}\right]^2 |\langle \vec{k}_1, c| e^{-i\vec{q}\cdot\vec{r}_1}|\vec{k}_1+\vec{q}, c\rangle|^2 f_{\vec{k}_1,c}(1-f_{\vec{k}_1+\vec{q},c})N_h(q), \tag{114}$$

where

$$N_h(q) = \sum_{\vec{k}_2} |\langle \vec{k}_2, v| e^{i\vec{q}\cdot\vec{r}_2}|\vec{k}_2-\vec{q}, v\rangle|^2 f_{\vec{k}_2,v}(1-f_{\vec{k}_2-\vec{q},v}) \tag{115}$$

and $f_{\vec{k}_2,v}$ is the probability that there is an electron in the state $|\vec{k}_2, v\rangle$. The valence-band mass is here assumed to be much larger than the conduction band mass, so that the process is elastic. This expression is formally identical to that for the probability of scattering by a random ensemble of ionized defects with $N_i Z_i^2 = N_h(q)$. However, $N_h(q)$ depends upon the statistics (availability of initial and final states) and symmetry properties of the valence band. An evaluation of $N_h(q)$ for a realistic distribution is extremely cumbersome and in any case cannot be included exactly in a scattering calculation; however, it is useful to examine two extreme cases to establish its limits.

We first consider the perfectly flat band case and restrict the momentum transfer to be small with respect to the dimensions of the Brillouin zone. For this case, all states are equally populated, and

$$f_{\vec{k}_2,v} = f_{\vec{k}_2-\vec{q},v} = (N-n_h)/N, \tag{116}$$

where N is the number of states per unit volume in the Brillouin zone. Since q is small,

$$|\langle \vec{k}_2, v| e^{i\vec{q}\cdot\vec{r}_2}|\vec{k}_2-\vec{q}, v\rangle|^2 \approx 1$$

over most of the zone, and one can easily show that

$$N_h(q) \approx n_h[1-(n_h/N)] \approx n_h . \tag{117}$$

This is the conventional result and depends upon having the holes distributed uniformly over a volume of the Brillouin zone of dimension much larger than the momentum transfer.

The other extreme case is that for which all the holes are localized in a pocket of radius k_h at the zone center:

$$f_{\vec{k}_2,v} = \begin{cases} 0 & (k_2 < k_h) \\ 1 & (k_2 > k_h) . \end{cases} \tag{118}$$

One can show for a $p^{3/2}$ valence band that

$$|\langle \vec{k}_2, v| e^{i\vec{q}\cdot\vec{r}_2}|\vec{k}_2-\vec{q}, v\rangle|^2 = \frac{1}{4}\left\{1+3\left[\frac{\vec{k}_2\cdot(\vec{k}_2-\vec{q})}{k_2|\vec{k}_2-\vec{q}|}\right]^2\right\}. \tag{119}$$

$N_h(q)$ is then given by

$$N_h(q) = n_h F(q/k_h), \tag{120}$$

where

$$F(v) = \frac{3}{8}\int_1^{1+v} dy\, y^2 \int_{(y^2+v^2-1)/2yv}^1 dx\left[1+\frac{3(y-vx)^2}{y^2+v^2-2yvx}\right] = \frac{105}{128}v - \frac{151}{256}v^3 + \frac{3^2}{2^7 v}[\ln(1+v)+(1-v^4)\ln|1-v|] + \frac{3^2 v}{2^5}[(\tfrac{3}{4}v^2-1)\ln(1+v)+(v^2-1)\ln|1-v|] - \frac{3^2 v^3}{2^6}[\ln(1+v)]^2 + G(v) \tag{121}$$

and

$$G(v) = \begin{cases} \dfrac{3^2 v^3}{2^5}\displaystyle\sum_{n=1}^{\infty}\frac{v^n}{n^2}\left(1-\frac{1}{(1+v)^n}\right) & (v \le 1) \\ -\dfrac{3^2 v^3}{2^5}\left[\dfrac{(\ln v)^2}{2} - \dfrac{\pi^3}{3} + \displaystyle\sum_{n=1}^{\infty}\frac{1}{n^2}\left(\frac{v^n}{(1+v)^n}+\frac{1}{v^n}\right)\right] & (v \ge 1) . \end{cases} \tag{122}$$

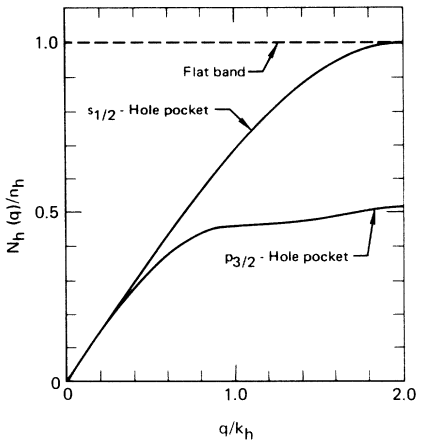

FIG. 12. The ratio of $N_h(q)$, the effective concentration of holes for scattering an electron through momentum transfer q, to n_h, the actual hole concentration, as a function of q/k_h where $k_h = (3\pi^2 n_h)^{1/3}$.

If the valence-band wave functions were free-electron- or s-like

$$(|\langle \vec{k}_2, v| e^{i\vec{q}\cdot\vec{r}_2} |\vec{k}_2 - \vec{q}, v\rangle|^2 = 1),$$

$F(v)$ would be given by

$$F(v) = \tfrac{3}{4}v - \tfrac{1}{16}v^3 . \tag{123}$$

The function $N_h(q)/n_h$, or $F(v)$, for the various cases is shown in Fig. 12. For the flat-band case $F(v)$ is, of course, constant and equal to 1. For the free-hole case $F(v)$ increases from zero at $q=0$ to 1 at $q=2k_h$. For the $p^{3/2}$-hole case $F(v)$ increases from zero at $q=0$ to a value of about 0.5 at $q=2k_h$. A uniform distribution of electrons in the hole pocket considerably increases the value of $N_h(q)$ near $q=0$, but increases $N_h(q)$ much less near $q=2k_h$.

This treatment, of course, ignores two other important problems: the applicability of the RPA dielectric function to screening of the electron-hole interaction,[52,53] and the accuracy of the Born approximation for electron-hole scattering. However, within these approximations, the contribution to the Boltzmann equation should be given by Eq. (105) with $N_i Z_i^2$ replaced by pn_h where p lies between about 0.5 and 1.0.

E. Calculation of the mobility

We write the Boltzmann equation for the steady state,

$$\left(\frac{\partial f(\vec{k})}{\partial t}\right)_F + \left(\frac{\partial f(\vec{k})}{\partial t}\right)_{\text{scat}} = 0 , \tag{124}$$

in the form of the finite difference equation

$$L(c') = rE_g^{3/2} s^3 e\mathcal{E} , \tag{125}$$

where

$$r = \hbar^2 \bar{M} v_a (2\mu_c' m_0)^{-3/2} (e_c^* e)^{-2} \omega_L / \pi \tag{126}$$

and

$$L = L_{\text{LO}} - \frac{\hbar^2 \bar{M} v_a \omega_L \lambda s E_g}{4\pi (e_c^* e)^2 \mu_c' m_0 f_0' \cos\theta} \left[\left(\frac{\partial f(\vec{k})}{\partial t}\right)_{\text{ac.}} + \left(\frac{\partial f(\vec{k})}{\partial t}\right)_{\text{i.d.}} + \left(\frac{\partial f(\vec{k})}{\partial t}\right)_{\text{e.h.}} \right] . \tag{127}$$

This equation is then solved with the variational method of Kohler[54] as modified by Howarth and Sondheimer[55] and Ehrenreich.[49] The function $c'(E)$ is expanded in a complete set $\{\phi_i(E)\}$:

$$c'(E) = \sum_{i=0}^{\infty} c_i \phi_i(E) . \tag{128}$$

The conductivity is then given by

$$\sigma = \bar{M} v_a \omega_L G / 3\pi^2 \hbar^2 (e_c^*)^2 , \tag{129}$$

where

$$G = \alpha_0^{(0)2}/d_{00} + \sum_{i=2}^{\infty} D_{\alpha 0}^{(i-1)} D_{\alpha 1}^{(i-1)} / D^{(i-1)} D^{(i)} . \tag{130}$$

The functions $\alpha_i^{(m)}$ and d_{ij} are defined by the relations

$$\alpha_i^{(m)} = E_g^{3/2} \int_0^{\infty} E^m s^3 \phi_i(E) f_0' dE \tag{131}$$

and

$$d_{ij} = \int_0^{\infty} \phi_i L(\phi_j) f_0' dE , \tag{132}$$

and $D_{\alpha n}^{(i)}$ and $D^{(i)}$ are the determinants

$$D_{\alpha n}^{(i)} = \begin{vmatrix} d_{00} \cdots d_{0,i-1} & \alpha_0^{(n)} \\ \cdot & \cdot \\ \cdot & \cdot \\ \cdot & \cdot \\ d_{i0} \cdots d_{i,i-1} & \alpha_i^{(n)} \end{vmatrix} \tag{133}$$

and

$$D^{(i)} = \begin{vmatrix} d_{00} & \cdots d_{0,i-1} \\ \cdot & \cdot \\ \cdot & \cdot \\ \cdot & \cdot \\ d_{i-1,0} & \cdots d_{i-1,i-1} \end{vmatrix} . \tag{134}$$

For the set $\{\phi_n\}$ we choose

$$\phi_n = (E/k_B T)^n . \tag{135}$$

The infinite series in Eq. (130) is carried out to second order. Random checks to tenth order indicate that higher-order terms contribute less than 2% to the total conductivity at all concentrations and temperatures.

VII. COMPARISON OF THEORETICAL AND EXPERIMENTAL MOBILITY

In this section the results of the variational calculation for normally behaving samples will be

presented. The deformation potential in HgSe is quite small, and we use a value[21] of 0.68 eV for E_0 and values of 0.45 for E_1/E_0 and 0.15 for E_2/E_0 given by the hydrogenic approximation. Deformation potential scattering is always masked by the other scattering processes; for example, the use of a value for E_0 of 2.5 eV (which is more consistent with the uniaxial-stress measurements of Seiler and Hathcox[56]) produces at most a change of 3% in the calculated electron mobility.

All of the samples, except 21*JB*, have 4.2 K mobilities lower than those predicted by scattering on singly ionized donors. Thus it is necessary to add additional defect scattering to account for the mobility deficit. The additional scattering may be due to either charged or neutral defects, and we will first consider the charged case.

Since the measured mobilities of some of the samples are less than half the values calculated from scattering on singly ionized donors, it is unlikely that doubly ionized donors are responsible for the deficit. We thus choose a simple model in which the samples contain singly ionized donors and singly ionized acceptors, the densities of which are adjusted to obtain agreement with the experimental mobilities at 4.2 K under the condition $N_D - N_A = n_e(4.2\ \mathrm{K})$. The defect densities substantially affect only the low-temperature results, the high-temperature calculations being dominated by LO-phonon scattering. The value of 9 for $\epsilon_\infty^t(300)$ was used, which gives values of 3.92 for e^* and 168 K for Θ_T. Theoretical curves calculated in this way for four of the samples are shown in Figs. 13 and

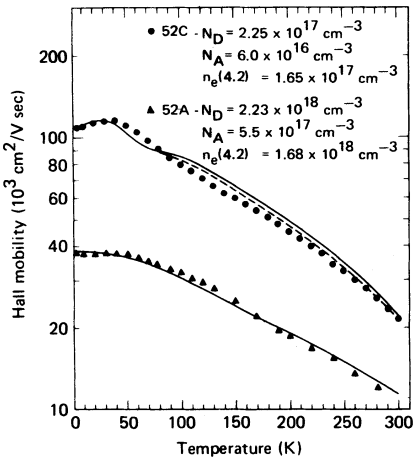

FIG. 13. Experimental and calculated electron mobilities in HgSe samples 52*A* and 52*C* for the case where ionized acceptors as well as donors are the principal scatterers at low temperature. The dashed curve for sample 52*C* is calculated for electron-hole scattering in the flat-band approximation and the solid curve for the approximation of a $p^{3/2}$-hole pocket.

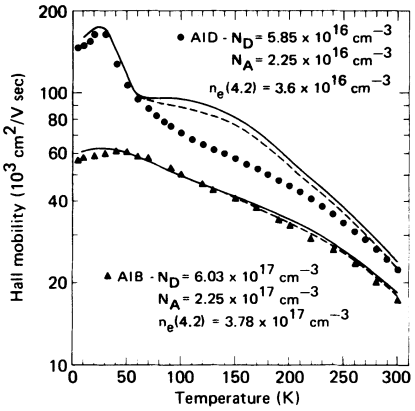

FIG. 14. Experimental and calculated electron mobilities in HgSe samples *AID* and *AIB* for the case where ionized acceptors as well as donors are the principal scatterers at low temperature. The dashed curve for sample *AID* is calculated for electron-hole scattering in the flat-band approximation and the solid curve for the approximation of a $p^{3/2}$-hole pocket. The rapid decrease in the mobility of sample *AID* between 30 and 50 K is due to interband scattering.

14 along with the experimentally measured values. The agreement is better than 10% in all samples except the very low concentration sample *AID*, for which the experimental values lie as much as 20% below the theory at medium temperatures (Fig. 14). Sample *AID*, being nearly intrinsic, is the only sample which has an appreciable hole concentration at medium temperatures, and the deviation may be due to an overestimate of the hole screening of the ionized defects. This sample is especially interesting because it clearly shows the rapid dropoff in mobility between 30 and 50 K arising from interband ($\Gamma_8^c \leftrightarrow \Gamma_8^v$) LO-phonon scattering and the change in slope between 75 and 100 K where intraband LO-phonon scattering begins to dominate. The generally good agreement between theory and experiment is gratifying since no attempt was made to adjust the parameters of the electron-LO-phonon interaction.

However, one feature of the results gives reason to doubt the validity of the ionized acceptor model. In Table III are shown the donor and acceptor concentrations for each sample required to fit the low-temperature data. Within each series of samples as the donor concentration was changed by annealing, it was necessary to correspondingly assume a change of the same magnitude in the value used for the acceptor concentration in order to fit the low-temperature data. We cannot construct a model of the defect kinetics which yields this result, that is, that the acceptor concentration increases nearly linearly with the donor concentration. However, a further analysis

TABLE III. Parameters for calculating the scattering of electrons by defects. The concentrations listed of donors N_D and acceptors N_A are required for the compensating-acceptor model. For the neutral-defect model a donor concentration equal to the 4.2-K electron concentration was assumed in addition to a mean-free-path Λ_0 associated with neutral scatterers.

HgSe sample	n_e (4.2 K) (10^{17} cm^{-3})	N_D (10^{17} cm^{-3})	N_A (10^{17} cm^{-3})	Λ_0 (10^{-4} cm)
AIB	3.78	6.03	2.25	1.8
AIC	1.89	3.09	1.20	2.0
AID	0.360	0.585	0.225	2.0
AIE	39.2	46.2	7.0	3.5
52*A*	16.8	22.3	5.5	2.3
52*B*	1.933	3.08	1.15	2.2
52*C*	1.65	2.25	0.60	3.0
52*D*	38.2	45.2	7.0	3.5
51*A*	17.8	21.3	3.5	5.0
51*B*	5.44	5.89	0.45	20.0
51*C*	5.70	6.60	0.90	6.0
51*D*	4.25	5.05	0.80	6.0
21*JB*	12.85	12.85	0	∞

of the scattering arising from the additional charged-defect concentrations shows that the mean free path associated with the extra defect scattering remains nearly constant within each series of samples. This leads us to the alternative hypothesis that the low-temperature mobility deficit is caused by scattering on neutral defects.

We can with some generality write for elastic scattering from neutral defects

$$\left(\frac{\partial f(\vec{k})}{\partial t}\right)_n = -\frac{f(\vec{k}) - f_0(E)}{\tau(E)} \tag{136}$$

and define the mean free time τ in terms of a mean free path Λ_0 and the electron velocity $v(E)$:

$$\tau(E) = \Lambda_0 / v(E) \ . \tag{137}$$

We further write Λ_0 as

$$\Lambda_0 = 1/N_0 d_0^2 \ , \tag{138}$$

where N_0 and d_0 are, respectively, the density and scattering length of the defects. This yields the contribution to the Boltzmann equation:

$$\left(\frac{\partial f(\vec{k})}{\partial t}\right)_n = \frac{2E_g s^3}{\hbar \Lambda_0 \lambda} c'(E) f_0' \cos\theta \ . \tag{139}$$

We now assume that d_0 is independent of electron energy and concentration, which is approximately true for a strong potential of dimension small with respect to k^{-1}, and that the scatterers are singly ionized donors of density $N_D = n_e(4.2\ \mathrm{K})$ and neutrals of density $N_0 = 1/\Lambda_0 d_0^2$. A slightly better fit is obtained by using a value of 9.75 for $\epsilon_\infty^t(300)$, which gives values of 9 for $\epsilon_b(300)$, 3.95 for e^*, and 173 K for Θ_T. Theoretical results, experimental data, and the fitted values of Λ_0 for all the samples with donor concentrations less than 2×10^{18} cm^{-3} are shown in Figs. 15–20. The fitted

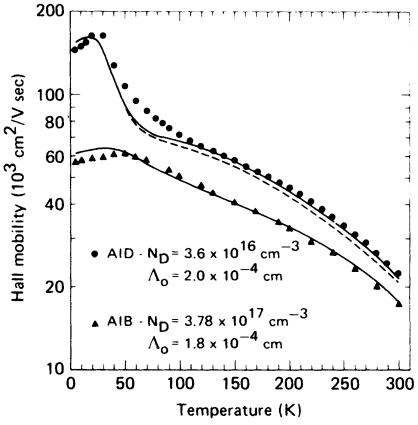

FIG. 15. Experimental and calculated mobilities in HgSe samples *AID* and *AIB* for the case where neutral defects and ionized donors are the principal scatterers at low temperature. The dashed curve for sample *AID* is calculated for electron-hole scattering in the flat-band approximation and the solid curve for the approximation of a $p^{3/2}$-hole pocket. The rapid decrease in the mobility of sample *AID* between 30 and 50 K is due to interband scattering.

values of Λ_0, shown in Table III, are nearly constant within each series (the value for sample 51*B* being an exception). If it is assumed that $d_0 = 5$ Å (approximately the unit-cell dimension), the mean free paths correspond to netural-defect densities ranging from less than 10^{17} to 2×10^{18} cm^{-3}. The mean free paths are thus compatible with the densities of neutral scatterers deduced from thermal-conductivity data for HgSe.[21]

For samples with impurity carrier concentrations below 2×10^{18} cm^{-3} (including sample *AID*), theory and experiment agree over the entire

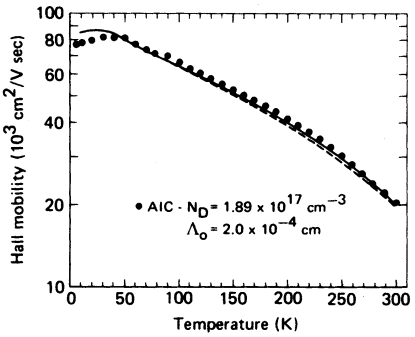

FIG. 16. Experimental and calculated electron mobility in HgSe sample *AIC* for the case where neutral defects and ionized donors are the principal scatterers at low temperature. The dashed curve is calculated for electron-hole scattering in the flat-band approximation and the solid curve for the approximation of a $p^{3/2}$-hole pocket.

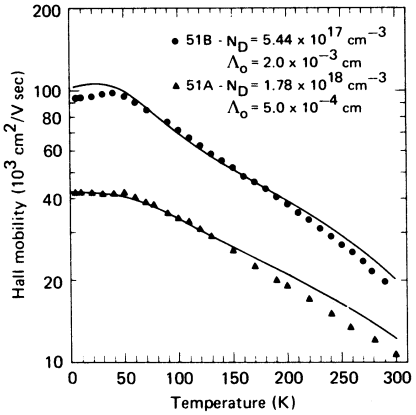

FIG. 17. Experimental and calculated mobilities in HgSe samples 51*A* and 51*B* for the case where neutral defects and ionized donors are the principal scatterers at low temperature.

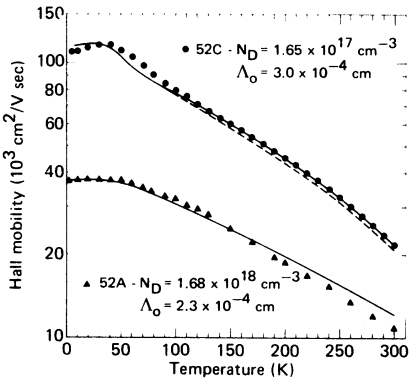

FIG. 19. Experimental and calculated mobilities in HgSe samples 52*A* and 52*C* for the case where neutral defects and ionized donors are the principal scatterers at low temperature. The dashed curve is calculated for electron-hole scattering in the flat-band approximation and the solid curve for the approximation of a $p^{3/2}$-hole pocket.

temperature range to within about 10%, with the largest deviations occurring at high temperature. Experimental and theoretical values of the mobility for two high-concentration samples ($N_D \approx 4\times10^{18}$ cm^{-3}) are shown in Figs. 21 and 22. As T increases, theory and experiment systematically diverge until at 290 K the data lie about 25% below the theoretical values. The beginning of a trend toward this behavior is already evident at an impurity concentration of 5×10^{17} cm^{-3}. As mentioned previously, the most probable reason for this discrepancy is the overestimate of the intraband screening of the electron–LO-phonon interaction as E_F becomes much larger than E_g, as is the case in the high-concentration samples at 290 K ($E_F/E_g \approx 5$). Such an overestimate is inherent in our use of the pure p function and parabolic band for the calculation of the q dependence of $\epsilon_e^{\text{intra}}$.

VIII. ANOMALOUS MOBILITY

The mobilities of two of the passive-annealed samples are shown in Fig. 23 along with the mobilities of two normally behaving samples with nearly the same electron concentrations. The mobility of each passive-annealed sample has an anomalous minimum at about 110 K. The anomaly appears to consist mainly of an increase in the mobility at about 110 K rather than a resonance-like behavior in the region between 50 and 140 K. No accompanying unusual behavior is observed in the Hall coefficient. When the temperature is

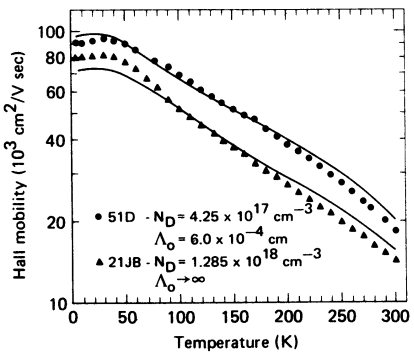

FIG. 18. Experimental and calculated mobilities in HgSe samples 51*D* and 21*JB* for the case where neutral defects and ionized donors are the principal scatterers at low temperature.

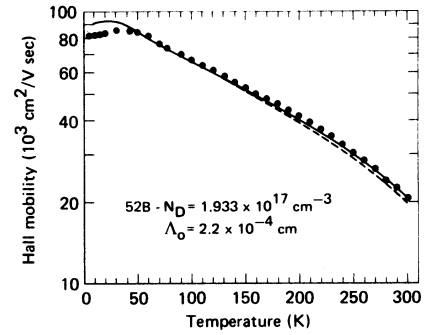

FIG. 20. Experimental and calculated electron mobility in HgSe sample 52*B* for the case where neutral defects and ionized donors are the principal scatterers at low temperature. The dashed curve is calculated for electron-hole scattering in the flat-band approximation and the solid curve for the approximation of a $p^{3/2}$-hole pocket.

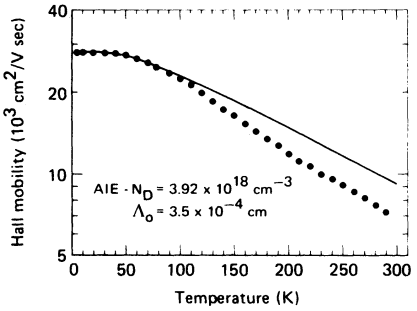

FIG. 21. Solid-line curve is the calculated electron mobility in HgSe sample *AIE*. For this high electron-concentration sample, the ratio E_F/E_g is large, and the consequent overestimation of the screening of the LO-phonon interaction gives a 25% too-large mobility value at 300 K.

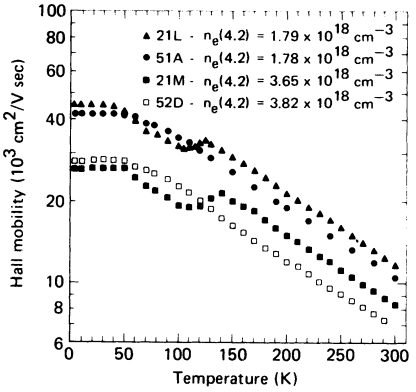

FIG. 23. Electron-mobility data shown are for two HgSe samples, 21*L* and 21*M*, which exhibit the anomalous mobility minimum, and for two normally behaving samples, 51*A* and 52*D*, which have nearly the same electron concentrations as the anomalous samples. In addition to having an anomalous minimum, the mobility for samples 21*L* and 21*M* is larger at high temperature than for the normal samples.

cycled between 4.2 and 300 K, the mobility anomaly is exactly reproduced. The anomalous-mobility samples are prepared by vacuum-annealing as-grown samples to achieve low electron concentrations, followed by passive annealing in air at room temperature during which time the electron concentration increases to relatively high values. The anomaly is never seen in samples with fewer than 10^{18} electrons/cm^3. Subsequent annealing in mercury vapor restores the samples to normal mobility behavior.

The increase in mobility at about 110 K cannot result from an increase in the screening produced by the Fermi level crossing the edge of either a normal perfect-lattice band (as in α-Sn) or an impurity band for two reasons: first, the temperature at which the increase begins is nearly independent of the Fermi level; and second, the Hall coefficient does not exhibit the anomalous behavior

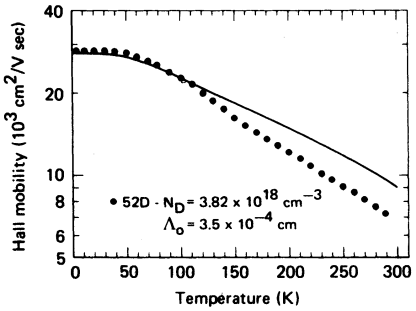

FIG. 22. Solid-line curve is the calculated electron mobility in HgSe sample 52*D*. For this high electron-concentration sample the ratio E_F/E_g is large, and the consequent overestimation of the screening of the LO-phonon interaction gives a 25% too-large mobility value at 300 K.

one would expect if another band were being populated. The possibility that a perfect-lattice band is involved is additionally ruled out by the fact that other samples with the same electron concentration do not exhibit the anomaly.

A decrease in the scattering beginning at 110 K because of deionization of some of the charged defects is also an untenable hypothesis because this too would produce anomalous behavior in the Hall coefficient. Although a change with temperature in the scattering cross section of neutral defects would produce no Hall anomaly, it also would not significantly affect the mobility near room temperature, where LO-phonon scattering is dominant. One observes in Fig. 23 that normal and anomalous mobility curves are nearly parallel at temperatures above the mobility maximum, and thus an explanation of the difference in mobility based upon some change in the neutral defect scattering is not satisfactory.

A remaining possibility is that the anomaly results from some defect-induced change in the temperature dependence of either the band parameters or the phonon frequencies. The possibility of an incipient phase-transformation was considered, but measurements in the mobility-anomaly temperature range of the intensity ratios of x-ray diffraction lines for several samples gave no evidence for this.

IX. DISCUSSION

The temperature dependences of the band parameters of HgSe have been deduced from Hall-

coefficient data. These band parameters, when used (along with measured optical and acoustical constants) in a microscopic theory of electrical conduction in zero-gap semiconductors, yield good agreement with the measured mobility data. However, at temperatures and ionized-donor densities such that $E_F/E_g \gg 1$, a systematic deviation between theory and experiment exists. A more accurate theoretical description of the mobility for this case would require an exact calculation of the intraband part of the electronic dielectric function. Such a calculation would be extremely useful, as would be a direct experimental determination of ω_T and the temperature dependence of ϵ_b.

From the analysis of the low-temperature mobility data, we conclude that the HgSe samples contain relatively large numbers of stable neutral defects, in agreement with the results of thermal conductivity experiments. The Szigeti effective charge,

$$e_s^* = 3e^*/[\epsilon_\infty^b(0)+2]\,,$$

has the high value 0.76 in HgSe as compared with 0.6 in HgTe.[38] Thus it may be that the Phillips-Van Vechten ionicity[31] f_i of HgSe is very near the maximum limit of f_i (0.785) for a stable zinc-blende lattice. This might explain both the unstable nature of the ionized defects as well as the large concentration of neutral defects frozen in during crystal growth. It is tempting also to speculate that the anomalous behavior of the passive-annealed samples is connected with the ionicity of HgSe being near the maximum limit for stable zinc-blende structures. Thus a further investigation of the native defects of this material would be of great physical interest.

ACKNOWLEDGMENTS

We are most grateful to Dr. S. Zwerdling and Dr. D. P. Ames for their support and encouragement during the progress of this work.

---

†Research conducted under the McDonnell Douglas Independent Research and Development Program.

[1]S. Groves and W. Paul, Phys. Rev. Lett. 11, 194 (1963).

[2]S. H. Groves, R. N. Brown, and C. R. Pidgeon, Phys. Rev. 161, 779 (1967).

[3]R. Zallen and M. L. Slade, Solid State Commun. 8, 1291 (1970).

[4]R. J. Wagner, E. D. Palik, and E. M. Swiggard, J. Phys. Chem. Solids Suppl. 32, 471 (1971).

[5]C. H. L. Goodman, Proc. Phys. Soc. Lond. B 67, 258 (1954).

[6]H. Gobrecht, U. Gerhardt, B. Peinemann, and A. Tausend, J. Appl. Phys. 32, 2246 (1961).

[7]M. D. Blue and P. W. Kruse, J. Phys. Chem. Solids 23, 577 (1962).

[8]T. C. Harman and A. J. Strauss, J. Appl. Phys. 32, 2265 (1961).

[9]E. O. Kane, J. Phys. Chem. Solids 1, 249 (1957).

[10]S. Groves and W. Paul, in *Proceedings of the Seventh International Conference on the Physics of Semiconductors* (Dunod, Paris, 1964), p. 41.

[11]T. C. Harman, W. H. Kleiner, A. J. Strauss, G. B. Wright, J. G. Mavroides, J. M. Honig, and D. H. Dickey, Solid State Commun. 2, 305 (1964).

[12]The absence of a direct gap would appear to produce a low-temperature instability toward exciton formation, but it is believed that the anomalous dielectric screening associated with $\Gamma_{8c} \longleftrightarrow \Gamma_{8v}$ excitations prevents a transition to an excitonic phase. The dielectric function leads to anomalous effects in the low-temperature transport, optical, and lattice-dynamic properties which have been extensively studied. For a recent review of this aspect of the zero-gap semiconductors, see: J. G. Broerman, in *Proceedings of the Eleventh International Conference on the Physics of Semiconductors* (Polish Scientific Publishers, Warsaw, 1972), Vol. 2, p. 917.

[13]J. G. Broerman, Phys. Rev. 183, 754 (1969).

[14]D. G. Seiler, R. R. Galazka, and W. M. Becker, Phys. Rev. B 3, 4274 (1971).

[15]C. R. Whitsett, Phys. Rev. 138, A829 (1965).

[16]A. I. Blum and A. R. Regel, Zh. Tekh. Fiz. 21, 316 (1951).

[17]I. M. Tsidil'kovskii, Zh. Tekh. Fiz. 27, 9 (1957) [Sov. Phys.-Tech. Phys. 2, 9 (1957)].

[18]M. Rodot and H. Rodot, Compt. Rend. 250, 1447 (1960).

[19]T. C. Harman, Phys. Rev. 118, 1541 (1960).

[20]T. C. Harman, J. Phys. Chem. Solids 25, 931 (1964).

[21]C. R. Whitsett, D. A. Nelson, J. G. Broerman, and E. C. Paxhia, Phys. Rev. B 7, 4625 (1973).

[22]A. Lehoczky, D. A. Nelson, and C. R. Whitsett, Phys. Rev. 188, 1069 (1969).

[23]J. G. Broerman, Phys. Rev. Lett. 24, 450 (1970).

[24]J. G. Broerman, Phys. Rev. B 1, 4568 (1970).

[25]J. G. Broerman, Phys. Rev. B 2, 1818 (1970).

[26]J. G. Broerman, Phys. Rev. Lett. 25, 1658 (1970).

[27]J. G. Broerman, Phys. Rev. B 5, 397 (1972).

[28]C. R. Whitsett and D. A. Nelson, J. Crystal Growth 6, 26 (1969).

[29]G. B. Wright, A. J. Strauss, and T. C. Harman, Phys. Rev. 125, 1534 (1962).

[30]R. R. Galazka, W. M. Becker, and D. G. Seiler, *Physics of Semimetals and Narrow-Gap Semiconductors*, edited by D. L. Carter and R. T. Bate (Pergamon, New York, 1971), p. 481.

[31]J. C. Phillips and J. A. Van Vechten, Phys. Rev. Lett. 22, 705 (1969).

[32]D. M. Marquardt, J. Soc. Ind. Appl. Math. 11, 431 (1963).

[33]B. L. Gelmont and M. I. Dyakonov, Fiz. Tek. Poluprov. 5, 2191 (1971) [Sov. Phys.-Semiconductors 5, 1905 (1972)]; Zh. Eksp. Teor. Fiz. 62, 713 (1972) [Sov. Phys.-JETP 35, 377 (1972)].

[34]S. S. Shalyt and S. A. Aliev, Fiz. Tverd. Tela 6, 1979 (1964) [Sov. Phys.-Solid State 6, 1563 (1965)].

[35]S. A. Aliev, L. L. Korenblut, and S. S. Shalyt, Fiz.

Tverd. Tela 7, 1673 (1965) [Sov. Phys.-Solid State 7, 1357 (1965)].

[36]C. R. Pidgeon and S. H. Groves, *II-VI Semiconducting Compounds*, edited by D. G. Thomas (Benjamin, New York, 1967), p. 1080.

[37]S. C. Yu, Ph. D. thesis (Harvard University, 1964) (unpublished).

[38]M. Grynberg, R. LeToullec, and M. Balkanski, Phys. Rev. (to be published).

[39]L. Liu and E. Tosatti, Phys. Rev. Lett. 23, 772 (1969); Phys. Rev. B 2, 1926 (1970).

[40]J. G. Broerman, L. Liu, and K. N. Pathak, Phys. Rev. B 4, 664 (1971).

[41]In Ref. 40 it is stated that use of the parabolic band and pure p-like wave function always leads to underestimates of the intraband screening. However, this is not generally true. For the case $E_F \gg E_g$, the s-p cross term $(\rho_1 x)$ appearing in the intraband matrix element $(|\langle \vec{k}, c | e^{-i\vec{q}\cdot\vec{r}} | \vec{k}+\vec{q}, c\rangle|^2 = \sum_{i=0}^{2} \rho_i x^i$, where x is the cosine of the angle between $\vec{k}$ and $\vec{k}+\vec{q}$) used in the calculation of $\epsilon_e^{\text{intra}}$ begins to dominate the p-p and s-s terms $(\rho_0 + \rho_2 x^2)$. This matrix element, which for the case $E_F \ll E_g$ is given by $\frac{1}{4}(1+3x^2)$, approaches the value $\frac{1}{4}(1+x)^2$ when $E_g < \Delta \ll E_F$. The effect of this change is to move the shoulder of the function $f_1(q)$ of Ref. 40, which provides the modification of the Fermi-Thomas screening appropriate to the wave-function symmetry, closer to $q=0$. For an interaction screened by the static dielectric function, this produces a negligible change in the scattering because of the large value of the static dielectric constant. However, it can produce an appreciable increase in the scattering for an interaction screened by the much smaller high-frequency dielectric function.

[42]J. Lindhard, Kg. Danske Videnskab. Selskab, Mat. Fys. Medd. 28, 8 (1954).

[43]H. Ehrenreich, J. Phys. Chem. Solids 8, 130 (1959).

[44]Z. I. Kir'iashkina, F. M. Popov, D. N. Bilenko, and V. I. Kir'iashkina, Zh. Tekh. Fiz. 27, 85 (1957) [Sov. Phys.-Tech. Phys. 2, 69 (1957)].

[45]V. V. Volkov, L. V. Volkov, and P. S. Kireev, Fiz. Tekh. Poluprov. 4, 1437 (1970) [Sov. Phys.-Semiconductors 4, 1230 (1971)].

[46]B. Szigeti, Proc. Roy. Soc. A 204, 51 (1950).

[47]E. Burstein, A. Pinczuk, and R. F. Wallis, in Ref. 30, p. 251.

[48]E. J. Moore, Phys. Rev. 160, 618 (1967).

[49]H. Ehrenreich, J. Phys. Chem. Solids 2, 131 (1957).

[50]W. Zawadzki and W. Szymańska, Phys. Status Solidi 45, 415 (1971).

[51]J. M. Ziman, *Electrons and Phonons* (Oxford U. P., London, 1963), p. 170.

[52]J. Kübler, Phys. Rev. 183, 702 (1969); in Ref. 30, p. 209.

[53]L. J. Sham and T. V. Ramakrishnan, in Ref. 30, p. 219.

[54]M. Kohler, Z. Phys. 125, 679 (1949).

[55]D. J. Howarth and E. H. Sondheimer, Proc. Roy. Soc. A 219, 53 (1953).

[56]D. G. Seiler and K. L. Hathcox, in Ref. 12, Vol. 1, p. 287.